PLASMA PROCESSING OF OILS USING A CORONA REACTOR

A Thesis

by

KALISSA ELSPETH ADKINS

Submitted to the Office of Graduate and Professional Studies of
Texas A&M University
in partial fulfillment of the requirements for the degree of

MASTER OF SCIENCE

Chair of Committee,	David Staack
Committee Members,	Kalyan Annamalai
	Maria Barrufet
Head of Department,	Andreas Polycarpou

December 2014

Major Subject: Mechanical Engineering

ABSTRACT

As the demand for energy grows, all available resources will have to be utilized. Heavy oils are one underutilized resource that represents 50% of all the oil resources, but only accounts for 10% of all oil production. Heavy oils are most valuable once they have been refined. Current methods of breaking long hydrocarbon chains include thermal cracking, coking, visbreaking, hydrocracking, and catalytic cracking. This thesis investigates an alternate process, specifically the ability of nonthermal corona plasma to crack heavy and extra heavy crude oil. Preliminary experiments determined the optimal electrode configuration and the temperature at which the oil should be processed in order to achieve a maximum current. These experiments were carried out in air at atmospheric pressure inside a fume hood. The variables considered were the number of high voltage points, the distance between the surface of the oil and the high voltage electrode, the depth of the oil, and the temperature of the oil. It was found that a higher temperature or a lower viscosity increased the conductivity of the heavy oil. A hexagonal multipoint high voltage electrode distributed the discharge over the cross sectional area of the oil while increasing the maximum current that could be applied to the oil before sparking occurred. The optimum distances for the multipoint-to-plane corona discharge were 30 mm between the electrodes and an oil depth of 15 mm. The preliminary experimental results were applied toward the final experimental determination of the cracking abilities of the corona reactor.

To capitalize on the fact that distillation towers are readily available in industry, one was constructed to contain the corona reactor. Distillation towers are used in refineries to separate different oil fractions by their boiling points. The entire tower was heated and the all the light condensates were separated from the heavy residue in a single batch process. The masses of the condensate and the residual were recorded to quantify the efficiency of the corona reactor in producing light oil. The corona discharge yielded more condensates than its control counterparts which were only thermally treated, however, the mass produced was often within uncertainty.

ACKNOWLEDGMENTS

I would like to thank my graduate advisor Dr. David Staack and my committee members, Dr. Kalyan Annamalai and Dr. Maria Barrufet, for their guidance and support throughout the course of this research. I would also like to thank Chevron for their funding of my research and education. Last but not least, I would like to thank my fellow researchers in the Plasma Engineering and Diagnostics Laboratory for their valuable input and assistance.

NOMENCLATURE

AC	Alternating current
AMU	Atomic mass unit
API	American Petroleum Institute
B_1	Beaker 1 located in base chamber of distillation column, contains heavy oil
B_2	Beaker 2 collects condensate formed from distillation tower
D_o	Depth of oil
D_p	Distance from oil surface to points of the high voltage electrode
D	Distance from ground electrode to high voltage electrode
DBD	Dielectric Barrier Discharge
DC	Direct current
HV	High voltage
I	Current
ℓ	Length of high voltage electrode point
n	Number of high voltage electrode points
PTP	Peak-trough phenomenon
R	Resistance
s	Spacing or distance between high voltage electrode points
SG	Specific gravity
t	Time

T	Temperature
V	Voltage
$\dot{V}$	Volumetric flow rate
V_B	Voltage at breakdown
VR	Vacuum residue

TABLE OF CONTENTS

Page

Page

Page

LIST OF FIGURES

Page

Page

Page

LIST OF TABLES

Page

1. INTRODUCTION

1.1 Background and Motivation

By 2040 it is expected that worldwide energy consumption will increase by 33 million barrels of oil per day [1]. To meet increasing energy demands, unconventional oil reserves are one viable option. Heavy crude oil compromises half of all oil resources, but currently only ten percent of that is actually used in production [2]. This is in part due to the added costs imposed by the current market, which necessitates the refining of crude oil into more valuable products. This includes processing the heavy oil into lighter and cleaner oil fractions in oil refineries. Before the heavy oil is even able to reach the refining plants, it is mixed with lighter oils and liquid petroleum gas (LPG) in an effort to lower its viscosity enough to be able to store it and transport it by pipeline [3].

The chemical composition of petroleum can drastically vary depending on the location and depth of the formation from which it was extracted. Petroleum can be composed of 83.0 to 87.0 percent carbon, 10.0 to 14.0 percent hydrogen, 0.05 to 6.0 percent sulfur, 0.05 to 1.5 percent oxygen, 0.1 to 2.0 percent nitrogen, and less than 0.1 percent of metallic compounds [4]. The presence of the metallic compounds can have a significant detrimental effect in the cracking process, especially with heavy oils in which there is a more concentrated amount. However, at the same time the metals increase the conductivity of the oil permitting a charge to be passed through it. Research with medium heavy crude oil (SG $\approx$ 0.9) has shown that the resistivity of the oil decreases exponentially with increasing temperature [5]. Many solid hydrocarbons are even semiconductors [5]. Residua have many similarities in composition to heavy crude oil.

However, they have a higher concentration of asphaltene, sulfur, nitrogen and metal compounds [6]. The conductivity of heavy oils, although still relatively low, and especially residua is one property that enables the possibility of the application of a plasma discharge for the refining of the oil.

1.2 Introduction to Nonthermal Plasma

A nonthermal plasma is an ionized gas in which the electron temperature is much greater than the ion temperature. It consists of active chemical radicals and other excited species which are known to accelerate reactions causing the formation of new stable compounds, similar to the effects of catalysts [7, 8]. This includes the ability of the plasma to enhance molecular dissociation and produce free radicals [9]. Where conventional catalytic cracking methods are unable to proceed due to the complex components in crude oils reacting negatively with the catalyst, plasmas are unaffected [7]. Neither do plasmas decay over time. Nonthermal plasmas can be used at atmospheric pressures, which allows for easier and less costly implementation in industry than low and high pressure options. They do not require long initiation periods and consume relatively low amounts of electrical power [7]. Unlike with thermal plasmas, the majority of the electrical energy goes directly into the plasma channel which initiates the chemical reaction; energy is not lost to heating. In addition, the nonthermal plasma does not require the same high temperatures that thermal cracking mechanisms need to initiate chemical reactions within the petroleum. Thus the amount of electrode erosion is lowered and less energy is consumed [10]. For these reasons,

nonthermal plasma technology has the potential to be an advantageous method of petroleum refining.

1.3 Thesis Objectives

The main objective of this thesis is to investigate the ability of a nonthermal corona discharge to crack long hydrocarbon chains. This includes determining the economic feasibility of the refining process developed. As such, the efficiency of the process must be maximized, both in terms of the energy efficiency and the amount of heavy oil converted to lighter oils.

1.4 Thesis Overview

Section 2 discusses in detail nonthermal plasma discharges, specifically the corona discharge. It provides a background of current hydrocarbon cracking techniques used in industry and notes recent activities in related research. Section 3 describes the general electrical circuit to create the corona discharge. It also provides the details of the set-up for the preliminary experimentations in the fume hood and the final experimentations in the distillation tower and lists several safety precautions. The results of the preliminary experimentations determining the electrode configuration and oil depth and temperature are described in Section 4. Based on these results, the distillation tower procedure and the effects of the corona reactor inside the tower were determined and inscribed in Section 5. Section 6 contains all concluding remarks about the heavy oil and corona discharge experiment, including the major findings and future recommendations. All supporting documents are attached in the Appendix.

2. DETAILED BACKGROUND AND LITERATURE REVIEW

2.1 Plasma

Plasma, as the fourth state of matter, comprises 99% of the known universe. It is so called because of the progression between the states of matter with increasing temperature. Just as an increase in temperature yields a change from a solid to a liquid, the energized molecules of a gas produces plasma. The increase of energy results in collisions within the gas causing the gas to become ionized. Several mechanisms of ionization include ionization by electron impact and photoionization. Plasmas are considered to be quasi-neutral in the fact that the electron and ion densities are approximately equivalent [11]. In order to be classified as a plasma the following conditions must be met:

1. the Debye length must be much smaller than the system dimensions,
2. the number of particles in a Debye Sphere must be much greater than one, and
3. the frequency of oscillations multiplied by the average time between collisions must be greater than one [12].

Plasmas can exist over a wide range of temperatures and pressures. They naturally occur in the form of the sun, lightning, and the aurora borealis. Both the sun and lightning are thermal plasmas. The aurora borealis is a nonthermal plasma.

The most common method of generating a plasma discharge is through an external electric field. The few naturally occurring electrons and ions present within a gas are accelerated by the electric field, causing them to collide with other molecules in the gas creating what is known as the avalanche effect [13]. As the avalanche propagates

between the anode and cathode, it amplifies the external electric field and forms a thin ionized channel or streamer between the electrodes [11]. With a high enough current the streamer creates a closed loop between the electrodes and a spark is produced. For a direct current external electric field different types of plasmas are generated as shown in Figure 1 as the voltage and current of the system are altered. The three main types are the dark discharge, the glow discharge, and the arc discharge.

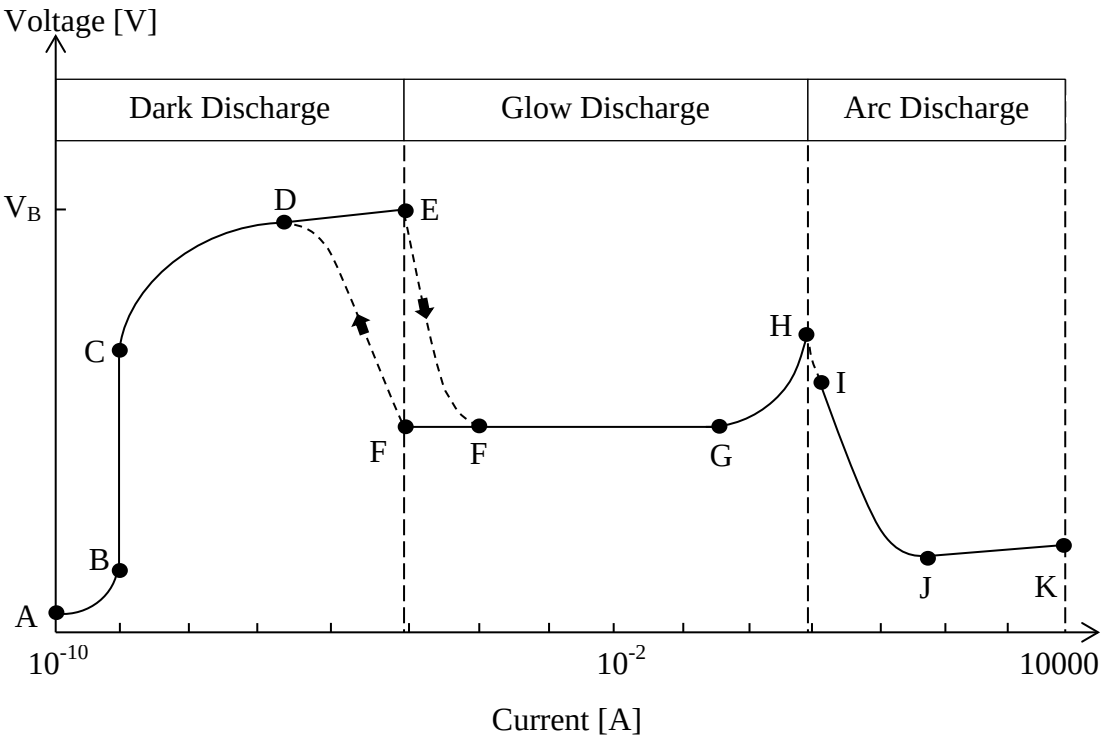

Figure 1: General current voltage characteristics for DC plasma discharge [11, 13]

The period from A to B is background ionization from cosmic rays. The dark Townsend discharge, which does not depend on the current and is self-sustained, is from C to E. D to E is the corona discharge. The transient period of breakdown of the corona discharge to the glow discharge from E to F is called a spark discharge; it begins at the breakdown voltage V_B. Electric breakdown is the process by which a dielectric material is changed into a conductor when the applied electric field is sufficiently strong [14]. The point at which breakdown of the plasma occurs is described by Paschen's curve for various gases. For each gas there exists a minimum breakdown voltage based on the electrode gap distance and the material used for the cathode. Pashchen's law shows that the voltage is a function of the similarity parameter *pd* [cm·Torr], which refers to the product of the gas pressure and the distance between the electrodes [14]. The normal glow discharge from F to G is independent of voltage and has a fixed current density. When the entire cathode is covered, an increase in the current results in an increase of the current density and the abnormal glow discharge (G to H). The abnormal glow to arc transition occurs from H to I. From I to J and J to K is the nonthermal arc and the thermal arc, respectively [11].

2.1.1 Thermal Plasma

A thermal plasma is one in which the electron temperature T_e and ion T_i or bulk gas temperature T_{gas} are in local equilibrium. The gas temperature is normally 18,000°F (10,000°C) or above. Some applications of thermal plasmas include arc welding, thermal plasma chemical vapor deposition, and tokamaks. However, in regards to plasma chemical reactions, thermal plasmas lack the ability to selectively treat the reactants.

Additionally, the high temperature causes overheating of the reactants which leads to energy inefficiencies [11].

2.1.2 Nonthermal Plasma

A nonthermal plasma has a higher electron temperature than ion temperature.

$$T_e > T_v > T_r \approx T_i \approx T_{gas} \tag{1}$$

The vibrational temperature T_v in Equation (1) is smaller than the electron temperature and larger than the rotational temperature T_r. The electron temperature is on the order of magnitude of 18,000°F (10,000°C) while the gas temperature can range from room temperature to 1500°F (800°C). The difference in temperature between the electron and ion arises from the variance in weight; because the electron is lighter it is able to move faster and has a higher collision rate [11]. For hydrocarbon cracking, rotationally and vibrationally excited molecules have too short of a lifetime and too low of energy (<2 eV) to be of use; the bonds between hydrocarbons normally falls between 3 and 6 eV. Instead, the chemical reactions occur as a result of electron-impact dissociation and ionization [15].

2.1.2.1 Dielectric Barrier Discharge

A dielectric barrier discharge (DBD) is a low-temperature discharge operable at atmospheric pressure. It is typically initiated by an alternating current (AC), has a voltage with an amplitude ranging from 1 to 100 kV, and a frequency up to several megahertz [16]. The discharge is formed between two parallel plate electrodes separated by one or more dielectric materials. The distance between the electrodes is usually on the

order of millimeters [17]. The DBD was first used in 1857 by Siemens to create ozone [11] and continues to be one of the most popular plasmas to use for plasma chemical reactions. In regards to organic compounds including hydrocarbons, it is limited by the complexity of the chemical reaction and a low product yield per unit energy input [17].This renders the DBD inefficient for large scale industrial operations.

2.1.2.2 Corona Discharge

The corona discharge has a lower electron density and higher breakdown voltage than the DBD [16]. A corona discharge appears around sharp edges and points with small radii of curvature where there is a sufficiently large electric field. It is considered a partial discharge in that the current flows from one electrode but does not reach the other. As such, the current is transferred by ions [18]. It emits a weak light that is strongest at the electrode with a high electric field. A positive corona is distinguished by a high electric field at the anode; a negative corona has a high electric field at the cathode. The negative corona propagates by impact ionization of the gas molecules [9].This thesis focuses on the positive corona discharge (see Section 2.1.4 and 2.3.2 for detailed explanation).

The positive corona depends largely on photoionization and forms when the ion density is large enough to extend the discharge into the inter-electrode gap [9, 19]. The positive corona has four phases dependent on increasing voltage. It begins with a burst pulse corona characterized by a concentration of light around the sharp point, steady current at a fixed voltage, and no sparking [9]. With increasing voltage and photoionization it develops into a noisy streamer corona that appears as a larger volume,

albeit still narrow channel reaching out from the anode toward the cathode [9]. During this phase the current is unsteady for a constant voltage. The ion temperature is in the hundreds of Kelvin [9]. The final two stages are the glow corona and spark, which is a high-temperature fully ionized plasma that connects the two electrodes. Transition to the spark is prevented by limiting the voltage, thereby creating a space charge accumulation around the sharp electrode [20] called the ionization region. The remaining discharge volume consists of a low electric field drift region that connects it to the cathode [21].

2.1.3 Liquid and Gas-Liquid Discharges

Traditionally plasma discharges have been created in gases. Liquid plasmas have also been studied extensively, although in most tests the liquid component has been water. Much of the information obtained from gas discharges can be applied to liquid discharges, but the actual method of discharge formation and propagation in the liquid is poorly understood. Plasma liquid reactions are dependent on the electrode geometry, electrode materials, presence of gas and liquid phases, and solution conductivity and composition. Electrohydraulic discharges are ones in which both electrodes are submerged in a liquid. In point-to-plane electrohydraulic corona discharges, when the large electric field is at the high-voltage electrode it causes extensive wear on the electrode, eventually making it incapable of sustaining a discharge. Studies of corona discharges in gases above water have shown that the conductivity of the water determines how the discharge channel propagates, the length of the channel, and the current. Compared to a pulsed arc, the corona discharge is more sensitive to the liquid solution conductivity. Furthermore, the gas phase affects the formation of gas-phase

species which then transfer into the liquid. If the liquid evaporates, it will in turn affect the gas-phase reaction. Radicals and other reactive species formed by the discharge may lead to post-discharge reactions. As of yet, there have been no studies analyzing the chemical reactions that occur at the gas-liquid interface for a corona discharge [18].

2.1.4 Plasma Chemistry

An important component of plasma is the chemical reactions that occur from the ionization process. The reaction components depend on both the gas and liquid mediums through which the plasma is formed. For the experiments within this thesis, the gas components are hydrogen (H_2) and methane (CH_4) and the liquid is a hydrocarbon. For a positive point-to-plane corona discharge, the neutral gas molecules ionize producing H^+, H_2^+, H_3^+, and CH_3^+, depending on the components of the original gas, as well as a free electron. The electrons are accelerated by the applied power preventing recombination. For the corona reactor developed herein, positively charged ions flow towards the ground electrode and the oil covering it. As the ions bombard the oil surface, hydrogenation of the heavy hydrocarbons occurs, effectively cracking the long chains into smaller ones and reducing the C/H ratio. Several types of chemical reactions involving the produced radicals are listed in Table 1. A radical is an unstable atom or molecule that has an unpaired electron such as CH_3, H, O, and OH [22]. The three main chemical reactions are initiation, propagation, and termination.

Table 1: Plasma induced chemical reaction pathways for hydrocarbon radicals [23]

Process	Chemical Reaction
Initiation	$e^- + CH_3CH_3 \rightarrow 2CH_3^{\bullet} + e^-$ $e^- + CH_4 \rightarrow CH_3^{\bullet} + H^{\bullet} + e^-$
Propagation – Hydrogen Abstraction	$CH_3^{\bullet} + CH_3CH_3 \rightarrow CH_4 + CH_3CH_2^{\bullet}$
Propagation – Decomposition	$CH_3CH_2^{\bullet} \rightarrow CH_2=CH_2 + H^{\bullet}$
Propagation - Polymerization	$CH_3CH_2^{\bullet} + CH_2=CH_2 \rightarrow CH_3CH_2CH_2CH_2^{\bullet}$
Termination – Hydrogenation	$CH_3^{\bullet} + H^{\bullet} \rightarrow CH_4$
Termination – Recombination	$CH_3^{\bullet} + CH_3CH_2^{\bullet} \rightarrow CH_3CH_2CH_3$
Termination – Disproportionation	$CH_3CH_2^{\bullet} + CH_3CH_2^{\bullet} \rightarrow CH_2=CH_2 + CH_3CH_3$

Chain initiation is the process by which a radical is formed from a stable species as a result of collisions with free electrons. Chain propagation has different radicals on the reactant and product sides of a chemical reaction; however the number of radicals remains constant. Through termination, the radicals recombine to form a stable product [22].

For a negative corona discharge, the electrons instead of the ions are accelerated towards the oil surface [24]. The indirectness of the process limits the amount of hydrocracking that takes place. Utilization of the positive corona discharge ensures that the hydrogen ions travel directly to the oil so a maximum amount of hydrocracking ensues.

2.2 Crude Oil

Oil is classified by the American Petroleum Institute (API) gravity which is related to the specific gravity *SG* of the oil at 60°F according to Equation (2) and has units of degrees.

$$API\ gravity = \frac{141.5}{SG} - 131.5 \tag{2}$$

The three generally accepted classifications of the oil types are listed in Table 2. A viscosity range is assigned in conjunction with the API gravity: extra heavy oil has a viscosity greater than 10,000 cP, light and heavy oil have a viscosity less than 10,000 cP at reservoir conditions [4]. The viscosity at 100°F is shown in Table 2.

Table 2: Oil classification based on API gravity [25, 26]

Classification	API Gravity [°]	Viscosity [cP]
Light Oil	>40	<10
Medium Oil	22.3-40	10-250
Heavy Oil	10-22.3	250-1300
Extra Heavy Oil	<10	>1300

Additionally, atmospheric residual oils typically have an API gravity ranging from 10° to 15° and the range for vacuum residua is 2° to 8° [4]. Oils with an API gravity greater than 10° float on water.

To become a useable product, the crude oil must be refined. This involves the separation of the various oil fractions, the conversion of heavier hydrocarbons to lights, and any subsequent finishing treatments [4].

Cracking is the process by which a long hydrocarbon chain is broken into smaller chains. A long hydrocarbon chain is one in which there are more of the relatively heavy carbon atoms (as compared to hydrogen), making it heavier than shorter chains with less carbon atoms. Hydrocarbons dissociate through either their C-C bonds or their C-H bonds. Dissociation of the C-C bonds leads to the formation of lighter hydrocarbons while dissociation of the C-H bonds results in the decomposition to hydrogen [27]. Typically the cracking of hydrocarbons involves high temperatures and pressures and chemical catalysts. Various methods include thermal cracking, catalytic cracking, visbreaking, hydrocracking, coking and gasification.

Thermal cracking is the application of heat for the lowering of petroleum viscosities. Often times it is used for the conversion of heavy oils and residua. The products produced depend upon the length of time the crude oil is held at a certain temperature. Visbreaking, or viscosity breaking, is a low temperature thermal cracking process carried out at 480°C (896°F) and 100 psi [4]. After a period of time at the high temperature, the product is quenched to prevent the formation of coke [6]. Coking is another thermal method. It can either be a continuous process as in fluid coking or the semi-continuous process of delayed coking [4]. In general, hydrogen is transferred from the heavy molecules to form lighter oil [6]. Coking produces gases, naphtha, fuel oil, gasoil, and coke and concentrates pollutants such as sulfur [4]. Delayed coking is able to

operate with any type of residua, however it has a high coke formation and low light oil yield [6]. Gasification completely cracks a residue into gaseous products. At temperatures exceeding 1000°C (1832°F), it produces syngas, carbon black, and ash as its major products and has therefore received less attention than other conversion methods [6]. With the addition of a catalyst, catalytic cracking can produce gas with a higher octane number and more of the stable iso-paraffins and aromatics than thermal process without a catalyst [4]. The range of operating temperatures and pressures is from 900 to 1000°F (482 to 538°C) and 1.5 to 3 atm respectively. As the demand for higher octane numbers has increased, catalytic cracking has replaced thermal cracking [28]. However, it can only treat oils with a high hydrogen to carbon ratio and low metal content, therefore it is limited to the treatment of atmospheric residue [6].

Hydroprocessing is based on the idea that the presence of hydrogen during the thermal reaction of the crude oil will terminate many of the coke forming reactions and promote the production of oil fractions with lower boiling points [4]. Hydroprocessing treats residues at low temperatures and high hydrogen pressures. Most of the time it involves a metal sulfide catalyst; the exception is for hydrovisbreaking which is visbreaking with the addition of hydrogen [6]. It can either be a destructive process where heavy hydrocarbons are converted to lighter ones, or a nondestructive process that improves the quality of the oil without altering its boiling point [4]. Although hydroprocessing has a high yield of light oil, it can be expensive. Thermal processes tend to be cheaper, but they do not have as high light oil yields, producing low-grade materials that require further refining [29].

A distillation unit is often used in conjunction with the cracking process. The purpose of this unit is to separate the different oil fractions based on the boiling points of the hydrocarbons. The typical range of boiling points is from 90°F (32°C) to over 800°F (427°C) [28]. This refining process begins with a desalting process to remove any salts which can cause fouling and corrosion of the equipment and deactivation of catalysts. From there the crude oil is heated in a furnace then flows into an atmospheric distillation unit. The bottom of the distillation unit has the highest temperature. As the oil evaporates and travels up the column the temperature is reduced; the lowest temperature is at the very top of the tower. The tower either is packed with a material that has a large surface area to increase mass transfer or contains 30 to 50 trays positioned at intervals that collect the various oil fractions as they rise and condense [4, 28]. The heavy oil residue left in the bottom of the tower, with a boiling temperature exceeding 343°C (649°F), is then transferred to a vacuum distillation unit with a larger diameter column [4, 6]. Vacuum distillation lowers the boiling point of the oil and enables separation at lower temperatures [4, 28]. The vacuum residua, with boiling temperatures greater than 565°C (1049°F), can be further refined in a coking unit [6, 28]. The energy required for atmospheric distillation is 658 Btu/yr.; for vacuum distillation it is 242 Btu/yr. [28].

This thesis will use a combination of the different cracking processes described above. The main reactor and chemical reaction initiator is the corona plasma discharge, which can be considered as a type of unconventional catalyst. It will also involve a form of non-catalytic (in the traditional sense of an additive material) hydroprocessing. A hydrogen rich gas will be used to attach to the long hydrocarbon chains as the chains are

cracked to both prevent the formation of coke and increase the amount of shorter hydrocarbon chains produced. Simultaneously to the corona and hydrogenation treatment, the crude oil will be heated in a distillation tower to separate the light and heavy oil fractions in a single batch process.

2.3 Research in Corona Discharge Configurations

There is limited literature concerning the cracking of heavy oil via corona discharges. As such, a number of different corona reactors lacking a heavy liquid oil component were studied with the assumption that the corona discharge would behave similarly regardless of experimental specifics. Each corona reactor is distinguished by its physical construction: point-to-point, point-to-plane, packed bed, and coaxial. They are further defined by the method in which they are generated: alternating current, direct current, or pulsed direct current [9]. There also exists a dependence upon the medium through which the plasma discharge flows, whether it is gaseous, aqueous, or a hybrid arrangement with only one electrode submersed in a liquid [30]. Knowledge gained from these studies aided in determination of the optimal configuration for the corona reactor evaluated within this thesis.

2.3.1 Electrode Geometry and Electrode Gap Distance

The classic method of generating corona discharges is between two asymmetric electrodes: a wire point and a plane electrode. Other geometries have been suggested, with emphasis on the type of electrode used for the high electric field. The material and dimensions of the points for different experiments are described in Table 3. When the

diameter of the wire used for the point is increased, the thickness of a plasma discharge is increased [24].

Table 3: Various point geometries in literature

Material	Diameter [mm]	Tip Angle [°] (Radius of Curvature [mm])	Length [mm]	Spacing [mm]	Source
Tungsten	0.5	30	10	5-20	[8]
Various metals & ceramics	0.75	-	15	-	[30]
Steel	0.6	(0.05)	>3	0-2.5	[31]
-	0.5	30	-	-	[32]
Thumbtack	-	(0.11)	5.5	25.4-27.0	[33]
Brass	-	(0.073-0.567)	5.5-25.5	-	[33]
-	1	(0.035, 0.095)	6		[34]
Stainless steel	0.5	30		20	[35]

Suarasan et al. experimented with the ozonization of liquids from two different multipoint AC corona discharge electrode geometries. The quantity of ozone produced depended on both the applied voltage and the duration of plasma exposure with a higher voltage yielding more ozone. Increasing the density of the discharge points increased the amount of ozone generated until a threshold of no significant effect was reached. Thinner liquid layers that were grounded and shorter electrode gaps also improved the ozone production [36]. The shorter electrode gap ensured that the entire space was filled with corona-induced plasma [9]. The various electrode gap distances for a number of

experiments are listed in Table 4. The first seven values are extracted from experiments that do not involve oil and are more focused on the electrode geometry.

Table 4: Distances between electrodes in literature

Inter-electrode Distance [mm]	Source
0-15	[8]
7	[9]
60	[30]
3-25	[31]
0-20	[32]
55.7-70.7	[33]
20, 31	[34]
15	[35]
3-15	[37]
2-10	[38]

Jaworek and Krupa determined the current-voltage characteristics of a grounded 5 by 5 square multipoint-to-plane corona discharge. Although results were similar to a single point discharge, the space charge interaction between adjacent points affected the VI trend. Increasing the spacing between the points and decreasing the distance between the electrodes increased the total achievable current and decreased the power per unit volume in the discharge gap [8].

Thanh evaluated a circular and linear arrangement of points for a negative corona discharge in air as compared to that of a single point with an inter-electrode spacing of 0 to 2 cm. It was found that the corona onset voltage had little dependence on the gap distance for gap lengths much larger than the radius of the point. The multipoint

electrode behaved similarly to a single point, but more charge was present in the electrode gap [32]. McKinney found that the maximum current achievable was unaffected by the length of a point for a fixed point tip-to-plane spacing. Longer points arranged closer together increased the area within the electrode gap that exhibited a current. Although sharper point tips drew slightly more current to a wider area, a corona could not be initiated for radii of curvature exceeding 0.567 mm. The presence of multiple points had no effect on the maximum current but did limit the distance over which it matched the Warburg distribution. Comparison between a square and hexagonal multipoint grid revealed that the hexagonal pattern had a more uniform current distribution [33]. Hoang et al. used a modified point-to-plane structure for a pulsed corona discharge reformation of ethane. A larger gap distance of 15 mm increased H_2 and CO selectivity, reduced the amount of byproduct hydrocarbons that formed, and had a better overall energy efficiency [37].

It is important to note that the use of any single electrode is limited due to the effects of erosion. Holzer and Locke investigated electrode erosion in a hybrid liquid-gas reactor. Regardless of material, all the point tips became rounded due to erosion from a corona discharge lasting for three hours [30]. As the electrode erodes, the discharge power is affected and the resulting debris most likely falls into the liquid. The least amount of erosion was observed for electrodes constructed from nickel chromium, thoriated tungsten, diamond-coated tungsten and stainless steel [30].

2.3.2 Negative vs. Positive DC Corona

Chen and Davidson compared the electron number density for the negative and positive corona discharge based on the linear current density, wire radius, and air temperature [24]. Although the negative corona produces more electrons than the positive corona, the electrons tend to be of lower energy and occupy a much smaller active volume [19, 24]. Increasing the gas temperature slightly lowers the number of electrons produced for a positive discharge and greatly increases the amount for a negative discharge. The voltage at which a corona discharge changes to a spark discharge is higher for the negative corona than the positive corona [24]. It is not possible to create a negative corona discharge in pure gases lacking any electron affinity [24]. This fact is further emphasized in that in pure H_2 an unstable negative corona discharge appeared at 2.6 kV and transformed into a glow discharge almost immediately at 2.8 kV [39]. The power per unit volume within the discharge gap is 2 to 3 times higher for a positive polarity than a negative one [8].

2.3.3 Aqueous/Gaseous Medium

Taghvaei et al. has shown that for a DBD oil cracker the carrier gas has a significant effect on the breakdown voltage. They found that although the breakdown voltage is increased with higher percentages of methane, the DBD could not be sustained in pure methane. The energy efficiency of the system also decreased with increases in methane [27]. This is explained by the different ionization potentials causing a mixed gas to have a greater degree of photoionization than a pure gas. The onset voltage for the corona is lower for pure argon, hydrogen and nitrogen than mixtures [39].

The performance of a corona discharge is affected by the pressure and the flow of the medium within the system. Chang et al. varied the gas flow rate of air in the region of a corona discharge from 0 to 20 L/min with an inlet gas temperature range from 10 to 60°C (50 to 140°F). They found that a flow rate stabilizes the corona discharge due to its cooling effect on the electrodes. Increasing the flow rate increased the voltage required to initiate the corona discharge and simultaneously increased the breakdown voltage while lowering the exit gas temperature [40]. Higher flow rates also decrease the amount of erosion on the point tips [30]. However, conversion of methane with a corona discharge decreased rapidly when the flow rate was increased [38]. Conversely, comparison of pressure effects from 5 to 15 psig at two different electrode gap distances showed that a higher pressure increased H_2 and CO production from ethane and reduced the amount of byproduct [37]. The onset voltage for the corona is lower for low pressures. As the pressure increased, the voltage required to sustain a constant current increased [39].

Jaowrek and Krupa varied the flow rate of air for a multipoint corona discharge within the laminar range. Similarly to Chang et al., they found that the corona is stabilized and the breakdown voltage is increased by 25% for a flow of 4 m/s as compared to stationary air. Too high of a velocity made it difficult to generate the corona discharge and extinguished preexisting coronas [35]. Chang, Lawless, and Yamamoto used a gas velocity of 100 m/s between a multipoint cathode and a plane anode. A significant amount of the gas bypassed the corona discharge due to the spaces between the points. They also report that a high-speed gas flow has a cooling effect on the

electrodes and stabilizes the plasma discharge for a corona torch, which in turn improves the chemical reactions [9].

2.4 Research in Reforming of Hydrocarbons

2.4.1 Thermal Cracking of Hydrocarbons

Although the experiment within this thesis does not seek to thermally crack crude oil, it does involve a heated distillation tower. To ensure that the light oils produced from the corona reactor are only from the plasma discharge and not due to the high temperature of the distillation tower, various thermal cracking experiments were researched with the main emphasis on the operation temperature. The thermal cracking of petroleum at temperatures below 1000°F (538°C) can be described by first-order kinetic equations. As the petroleum is heated, the thermal energy is applied toward cracking large hydrocarbon molecules into smaller fragments [3].

Tests involving the direct heating of methane were performed by Abánades et al. to determine the amount of hydrogen that could be produced. Lower flow rates did not require as high a temperature as high flow rates to produce hydrogen. As the temperature was increased from 875 to 1065°C (1607 to 1949°F), the amount of hydrogen increased, reaching a maximum conversion rate of about 30%. At temperatures exceeding 1350°C (2462°F) the residence time was negligible due to the faster reaction kinetics, but the system was limited by the formation of a carbon plug. Even with long residence times, the formation of hydrogen and carbon are low at temperatures below 1100°C (2012°F) [41]. Henderson and Weber determined that temperatures below 500°F (260°C) are too slow to be practical for thermal cracking of heavy crude oils [3]. It is not until a

temperature of 660°F (350°C) has been reached that the thermal cracking of oil becomes significant [4]. Above 700°F (371°C) the rate of coke formation increased, especially at high pressures [3]. The thermal cracking of heavy Marlim vacuum residue (VR) was carried out in 1 MPa of nitrogen gas. The system was heated to a reaction temperature of 400 to 440°C (752 to 824°F) at a rate of 10°C/min and held there for 0 to 90 minutes. As seen in other experiments, increases in both temperature and treatment time increased the amount of hydrogen produced [42].

Coking is another thermal treatment commonly used in the upgrading of petroleum. The vacuum residue of a Nigerian medium crude oil with an API gravity of 11.9° was thermally cracked in a delayed coker with temperatures up to 600°C (1112°F) and residence times ranging from 0 to 120 minutes. The liquid products were composed of 49.1 wt.% aliphatic hydrocarbons, 23.5 wt.% aromatic hydrocarbons, and 12.4 wt.% naphthenic hydrocarbons [43].

2.4.2 Plasma Cracking of Hydrocarbons

There has been some research involving the plasma cracking of hydrocarbons. A large portion of that research has been done with the goal of producing hydrogen from lighter hydrocarbons such as methane, propane, kerosene, and ethanol with a limited number producing hydrogen from heavy hydrocarbon cracking [27]. A limited number of papers have explored the possibility of applying plasma to crack medium and heavy oils.

The most widely used plasma that has been applied in the breaking of hydrocarbon chains is the dielectric barrier discharge. DBD cracking of hydrocarbons

has been investigated by [27], [38] and [44-49]. Prieto et al. used a packed-bed plasma reactor consisting of two mesh electrodes separated by 0.50 to 3.00 cm with an argon flow rate of 50 to 400 mL/min and input power ranging from 5 to 25 W [46]. A DBD with an open gap between two dielectric walls had no noticeable difference in methane conversion than a packed pellet-bed DBD [38]. When the applied voltage was increased the production of light hydrocarbons increased [44, 47, 50]. Experimenting with the setup proved the best results were at 7 kV and 18 kHz for a feed injection rate of 1 mL/min. With an input power requirement of 24.7 W, the maximum generation of gas from naphtha was 22.5 mL/min [44]. Khani et al. also studied the dependency of the reaction on the setup parameters, but for n-hexadecane. The conversion of oil increased from 2.63% to 3.85% and the cracking percentage increased from 40.72% to 64.15 % with a switch in the type of working gas from air to methane. Although it was believed a high flow rate would decrease the residence time of oil molecules within the plasma zone, increasing the flow rate from 10 to 50 mL/min produced a greater number of electrons, ions, and radicals leading to the higher conversion percentage of 9.41% [47]. A Brazilian heavy crude (API gravity 10.1) containing emulsified water in combination with various gases was treated for up to 4 hours at 13 kV and 65°C (149°F) by Honorato et al. Although there was a significant reduction in the viscosity of the DBD-treated oil, it was accompanied by a substantial loss of water; there were no important alterations in the ratio of hydrogen to carbon [45]. Renneke et al. and Rosocha et al. were able to crack ethane into H_2, CH_4, C_2H_2, and C_2H_4. They found that higher temperatures led to larger concentrations of the aforementioned molecules [48, 49].

A variety of corona discharges have also been tested. Marafi and Lobban (as well as Hoang et al.) tested the ability of a DC corona discharge to crack ethane, finding that the positive corona had a higher electron concentration and was more stable than a negative corona [19, 50]. Furthermore, a higher temperature increased the ionization rate and subsequent chemical reaction rate [50]. When Li et al. used a DC corona reactor with a feed flow rate of 60 mL/min and a discharge power of 45 W, they discovered that the H_2/CO ratio in the products strongly depended on the CH_4/CO_2 ratio in the feed. Moreover, when the CH_4/CO_2 ratio was greater than 2/1, coke deposits appeared on the cathode [19]. In an AC point-to-plane corona reactor, methane conversion, predominantly to acetylene, was increased from 67% to 72% with reduction in flow rate from 20 mL/min to 10 mL/min [38]. The wire-cylinder pulsed corona of van Heesch et al. reformed the heavy tar components of thermally generated biogas in pure nitrogen at gas temperatures ranging from 103 to 170°C (217 to 338°F). At an energy density of 161 J/L, 68% was converted and the light tar fraction increased by 50% [51].

Yang compared the ability of a packed DBD reactor and an AC point-to-plane corona discharge at processing methane. The main product from the DBD was ethane while the corona produced acetylene. With the same input energy, the corona discharge was able to convert more methane than the DBD, but both reactors had a larger yield for higher power inputs and longer residence times [38].

Other plasma cracking mechanisms involve the plate-to-plate, gliding arc discharge, microwave generated plasmas, and electron beams. Prieto et al. tested a steel mesh plate-to-plate reactor with an electrode gap distance ranging from 3 to 10 mm. The

highest production of light oil was at the largest gap distance (10 mm) and the lowest input power (3 W) [52]. There was a strong interaction between the flow rate and gap distance and the input power and gap distance. A maximum efficiency of 70 μL/J was achieved for the large gap distance of 0.9 cm and low input power of 5 W [53]. Matsui et al. experimented with two plates separated by 62 mm and filled with a mixture of 100 mL of one of four different types of oil and metal chips. The chips decreased in size during treatment and their shape had little influence on the rate and concentration of the generated gases. Although, two times more hydrogen was produced for an aluminum chip than a copper one [54]. Gallagher et al. tested the n-tetradecane reformation ability of two gliding arc systems, one with a reverse vortex flow. The reactors had nearly identical yields of partial oxidation of the heavy hydrocarbons to syn-gas with 50% efficiency and a byproduct of other light hydrocarbons [10]. Miknis et al. used a microwave plasma to convert a crude oil with API gravity of 23.1° and scrap tires in combination with hydrogen or methane. The tire had a 53% conversion rate to gas and liquid products. For the oil and methane, around 10% of the methane was converted to liquids via recombination reactions [55]. Hueso et al. used a microwave plasma in conjunction with water to convert heavy, highly aromatic oil and coke. The composition of the product varied based on the treatment time, but in general it included syngas and hydrogen and the sulfur content was reduced. For the heavy oil, the input energy requirement was 120 kJ/g and for the solid coke it was 180 kJ/g [56]. Electron beam treatment of asphaltene has led to the decomposition of the heavy hydrocarbon

molecules and reduction of the aromatic components. However, the penetration depth of the electron beam into the oil is limited [57].

3. EXPERIMENTAL DESIGN

3.1 General Setup

3.1.1 Electrical Circuit

A corona discharge is created near sharp points when the electric field between a high voltage (HV) electrode and a ground electrode is sufficiently high. In these experiments a direct current (DC) was used to generate a positive corona discharge. The general circuit for the corona discharge is shown in Figure 2.

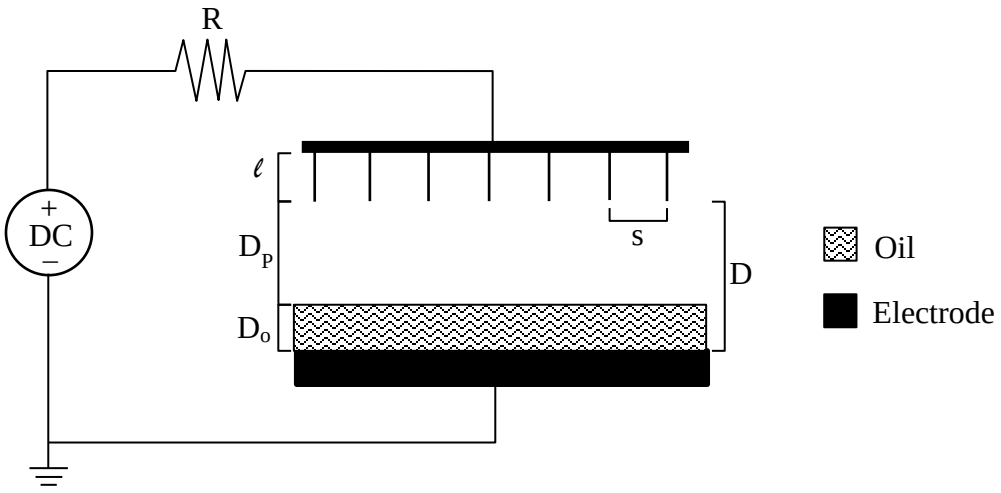

Figure 2: Corona discharge electrical circuit

A Spellman SL 10W-300W high voltage power supply provided the DC input power into the circuit. The power supply was connected to a ballast resistor bank. Unless stated otherwise, for the majority of the experiments the resistor bank consisted of ten 20 MΩ

resistors connected in parallel, yielding a total resistance R of 1.97 MΩ. The resistor bank was connected to the high voltage electrode. The high voltage electrode consists of n number of points of length ℓ with a spacing of distance s between each point. Unless otherwise stated, the points are constructed of 18 AWG bare nickel chromium. Each point tip was cut to an angle of 45° with an angle length of approximately 0.65 mm (Figure 3). The points are attached to a steel mesh, which allows the flow of gases to and from the beaker. The ground electrode is located a distance D from the tips of the HV points. D is composed of the depth of the oil D_o and the distance between the surface of the oil and the HV points D_p. The ground electrode and the power supply are connected to ground.

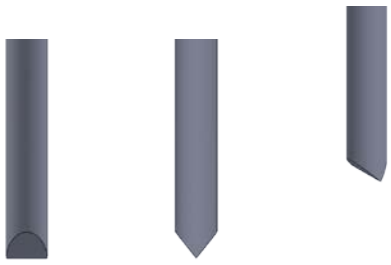

Figure 3: 45° cut of tip of high voltage points

3.1.2 Preliminary Experimental Setup

Preliminary experiments were executed in a fume hood in air at atmospheric pressure following the electrical setup as described in Section 3.1.1 with the general arrangement shown in Figure 4. The HV electrode is suspended over the oil by an optical stand. For these tests, oil c and oil d are used. Both are heavy oils however, oil d has a higher viscosity and lower API gravity than oil c. The beaker is 250 mL and the ground electrode has a height 59.66 mm and a diameter of 16.35 mm. The beaker is heated from below by a Thermolyne Cimarec 3 hot plate stirrer.

Figure 4: General configuration for corona treatment of heavy oil

The power supply voltage and current are measured according to the values displayed by multimeters attached to the terminals on the back of the power supply. The multimeters provide a greater degree of accuracy than the power supply display. The actual voltage is determined from a combination of the ballast resistor $R_{ballast}$ described in Section 3.1.1, the oil resistance R_{oil}, and the resistance of the plasma discharge R_{plasma} as follows.

$$V = R_{ballast}I + R_{oil}I + R_{plasma}I \tag{3}$$

I is the electrical current. The oil resistance can be approximated by

$$R_{oil} = \frac{D_o}{A\sigma(T)} \tag{4}$$

where A is the cross sectional area of the oil and $\sigma(T)$ is the electrical conductivity of the oil as a function of the oil temperature. This assumes that the oil is a long cylinder with terminals at each end [58]. The plasma resistance is a function of the current and the length of the plasma L_{plasma}. Equation (3) then becomes

$$V = R_{ballast}I + \frac{D_o}{A\sigma(T)}I + R_{plasma}(I, L_{plasma})I \tag{5}$$

Taking the partial differential of the voltage with respect to the oil depth yields

$$\frac{\partial V}{\partial D_o} = \frac{I}{A\sigma(T)} \approx \frac{\Delta V}{\Delta D_o} \tag{6}$$

The change in the oil depth refers to the instantaneous fluctuations in the oil depth created by the corona discharge. ΔV is the change in voltage from the surface of the oil to its full depth (function of the thickness of the oil). The effective area *Aσ(T)* can then be determined.

$$A\sigma(T) = \frac{\Delta D_o}{\Delta V} I \tag{7}$$

The optimal electrode configuration is chosen when this effective area is maximized. Although the instantaneous depth of the oil was unable to be measured, the ramifications were observed in the preliminary experimental results by the change in current with fluctuating oil depths. The optimal electrode configuration was quantified by the highest current achievable before sparking occurred.

3.1.3 Distillation Tower

A distillation tower was built to separate the lighter oils from the heavy oils. See Figure 5 for details. The distillation tower originally consisted of a lower base chamber with an outer diameter of 30 cm and height of 20 cm, and a column with an outer diameter of approximately 40 mm and height of 85 cm. In later tests beginning on 7.25.14, the column was replaced with one with a height of 16 cm and a diameter of 0.64 cm. A graphite gasket seals the lid of the base chamber, to which the column is attached. Sixteen bolts secure the lid to the base chamber. The lid of the base chamber has four holes: two are for the HV wire and ground wire, one is for the base chamber temperature probe16.1 which measures T_1, and the last one is the gas inlet. The HV wire is fed through the lid with an industrial spark plug. The volumetric flow rate of the inlet gas is

controlled by an Alicat Scientific M-series mass flow meter. The chamber and column are insulated with a layer of fiberglass and covered by sheet metal.

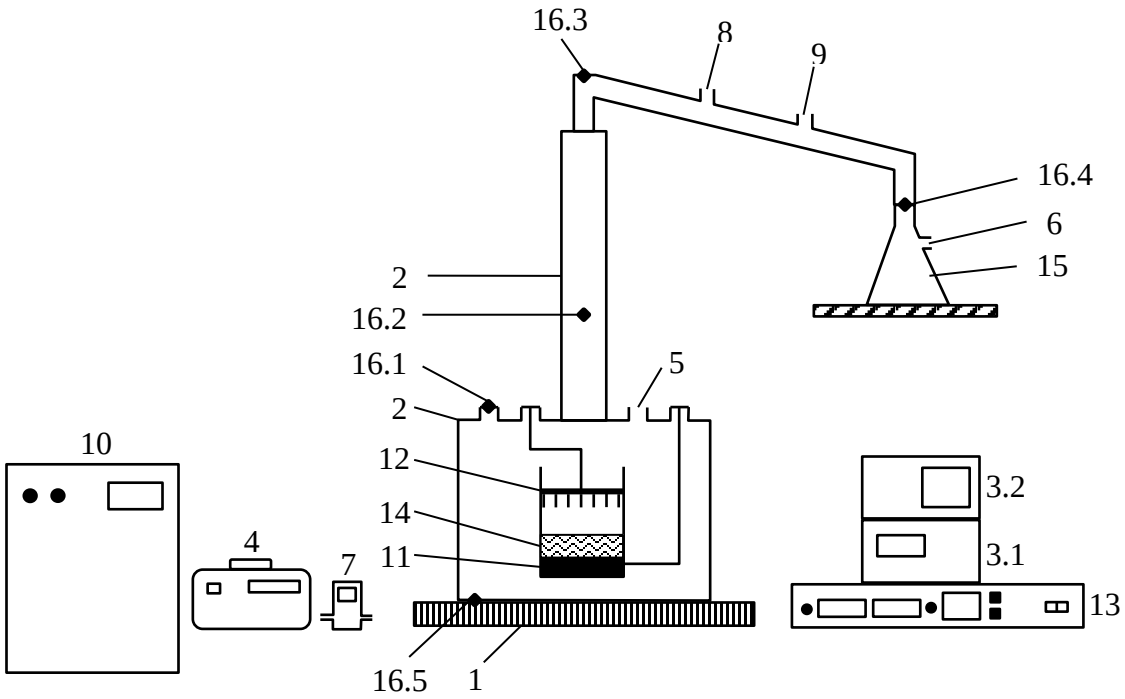

1. Hot plate
2. Heat tape
3. Heat controller
4. Variac transformer
5. Gas inlet
6. Gas outlet
7. Gas flow meter
8. Coolant inlet
9. Coolant outlet
10. Recirculator
11. Ground electrode
12. High voltage electrode
13. Power supply
14. Crude oil
15. Condensate collector (B_2)
16. Temperature probes

Figure 5: Distillation tower and experimental apparatus

Within the base chamber is a 250 mL beaker (B_1) layered with a ground electrode, heavy oil, gas, and a high voltage electrode. These components form the electrical setup as shown in Figure 2. For these tests only oil d is used. The ground electrode has a height of 59.66 mm and a diameter of 16.35 mm. The internal wires are insulated with a combination of Kapton® tape, fluorosilicone rubber tubing, ceramic tubing, and ceramic sleeving. The internal system can be viewed in Figure 6.

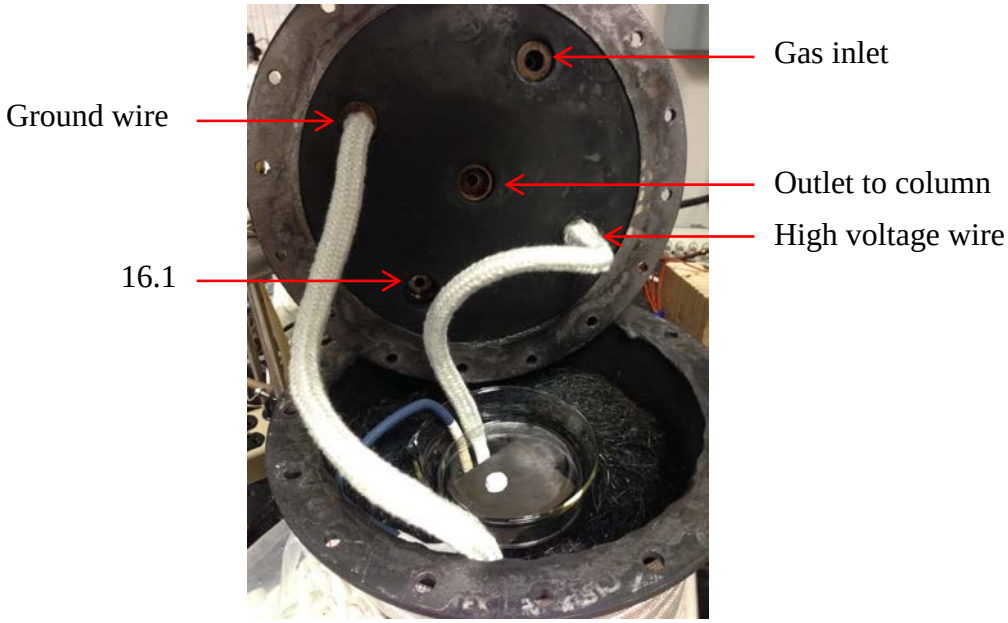

Figure 6: Internal configuration of the distillation tower

The high voltage electrode is suspended from a ceramic block resting on the rim of B_1. This beaker is located inside of a 1000 mL beaker and covered with a petri dish in order

to contain the electrical discharge. Steel wool is in the bottom half of the base chamber surrounding the 1000 mL beaker to facilitate the process of heat transfer. For the 85 cm column, steel wool is also located along the inside of the column. Tubing extends from the top of the column and into a beaker (B_2) and is cooled by a VWR Refrigerated Recirculating Chiller. The change in temperature results in the condensing of any of the lighter oils that vaporized in the base chamber. The downward angle of the tubing enables the flow of the condensates into B_2. A tube is connected to B_2 and exhausts gases into an overhead vent.

The entire distillation tower is heated. The base chamber rests on a Cimarec ™ Digital Stirring Hotplate controlled by internal temperature T_{HP}. The sides of the base chamber are covered with 3 HTS/Amptek Duo-heating tapes (8 ft., 624 W, 78 W/ft., 5.2 A). The temperature of the base chamber T_1 is monitored by a PXR3 Micro-Controller and switched by a Watlow E-Safe II relay (see 3.1 in Figure 5) based on the input of temperature probe 16.1. The lower half of the column has one HTS/Amptek Duo-heating tape (8ft, 624 W, 78 W/ft., 5.2 A) manually controlled by a variable AC (variac) transformer (TDGC-2KM) based on the temperature T_2 of probe 16.2. The upper half of the column has one heat cable (6 ft., 468 W, 78 W/ft., 3.9 A) regulated by heat controller 3.2 (Extech 48VFL11) based on the temperature T_3 of probe 16.3. The temperature T_4 is only monitored and not controlled. All of the heat tapes have a maximum operating temperature of 1400°F. Temperature probe 16.1, 16.3, and 16.4 (T_4) measure the internal temperature of the system while 16.2 measures the external temperature of the column

and 16.5 (T_5) measures the external temperature of the bottom of the base chamber. All of the temperature probes are Type K thermocouples.

3.2 Safety Precautions

For each of the substances described below, refer to their respective material safety data sheets (MSDS).

3.2.1 Petroleum

These experiments were conducted with various types of crude oils. Crude oils are amber to black liquids with mild to pungent sulfurous odors. They are flammable both in liquid and vapor form, with a lower and upper flammability limit of 1.4% and 7.6% by volume in air, respectively. Auto ignition occurs at 280°C (536°F). Complete combustion forms carbon dioxide, water vapor, and possibly oxides of sulfur and nitrogen; incomplete combustion may produce carbon monoxide. Crude oils may release hydrogen sulfide gas (H_2S) which is a corrosive, flammable, and highly toxic colorless gas that is characterized by a rotten-egg odor. If high viscosity oil is swallowed, it can be harmful; the oil can enter the lungs causing severe injury and even death. Prolonged skin contact with or breathing petroleum may cause cancer.

When dealing with petroleum it is vital that precautionary steps be taken. The work area must have adequate ventilation. Gloves must be worn while handling any oil. It is also recommended to wear lab coats and safety glasses when adequate protection is not provided by the general experimental setup. If any oil gets on the skin, the affected area should be immediately washed with soap and water. Used oil must be disposed of as a hazardous chemical waste. Where feasible, air inside the test chamber should be

purged with an inert gas (in this case nitrogen was used), especially when the oil is subjected to high temperatures. When this is not an option, some means of smothering the flames should be kept nearby in case of ignition; water must not be used as it will cause the oil to splatter and explode.

3.2.2 Hydrogen Gas

Several of these experiments were conducted using hydrogen gas. Hydrogen is an extremely flammable gas in the presence of oxidizing materials, including air. As such, it has the possibility of igniting with an invisible flame when its concentration is between 4% and 76% by volume in air. Auto-ignition occurs at temperatures ranging from 500°C to 571°C (932 to1060°F). In addition, hydrogen is an asphyxiant and may cause damage to the lungs. When under pressure, hydrogen gas is extremely cold and contact with this gas while it is rapidly expanding can result in burns or frostbite.

Precautionary measures should be taken while handling hydrogen gas. A hydrogen gas detector should be placed within the work area to alert personnel of concentrations greater than 200 ppm. The room must have adequate ventilation. A back flow preventive device should be connected to any tubing. Valves should be opened only once tubing is fully connected and should be closed after each use. To prevent ignition, air should be purged with an inert gas prior to initiation of hydrogen flow and before the experimental chamber is opened. For these experiments, nitrogen was used as the inert gas.

4. PRELIMINARY EXPERIMENTAL RESULTS

4.1 Electrode Geometry

The focus of these tests was to determine the optimal parameters for the set up that would result in the highest possible current for the corona discharge. Various HV point geometries were evaluated. For each electrode configuration, the independent variables were the depth of the oil, the distance from the high voltage points to the surface of the oil, and the temperature of the oil. The temperature was measured by placing a K-type thermocouple within the oil. When the power supply was on, the thermocouple wire was removed to prevent a discharge to the wire.

4.1.1 High Voltage Points

Oil c was evaluated at approximately 100°C (212°F) in air at atmospheric pressure inside a fume. The tendency of oil c to expand at this temperature was taken into account while positioning the HV electrode. The aluminum ground electrode had a height of 59.66 mm and a diameter of 16.35 mm. D_o was set at either 10 mm or 20 mm while D_p was set at either 10 mm or 15 mm. The voltage was incrementally increased, and the voltage and current (VI) were recorded from a set of multimeters connected to the power supply. Data was no longer recorded once a spark appeared. Three different HV point geometries, including a single center point, four linear points, and 19 points distributed in a hexagonal pattern were considered.

4.1.1.1 Single HV Point

The standard single high voltage point-to-plane ground electrode was evaluated first. The point was an 18 AWG bare nickel chromium wire with the tip cut to a 45°

angle. The VI trend can be seen in Figure 7. When D_o and D_p were increased, a higher voltage was required to reach the same current values obtained at lower distances. The maximum current obtained before sparking was 0.068 mA for D_o=10 mm and D_p=15 mm.

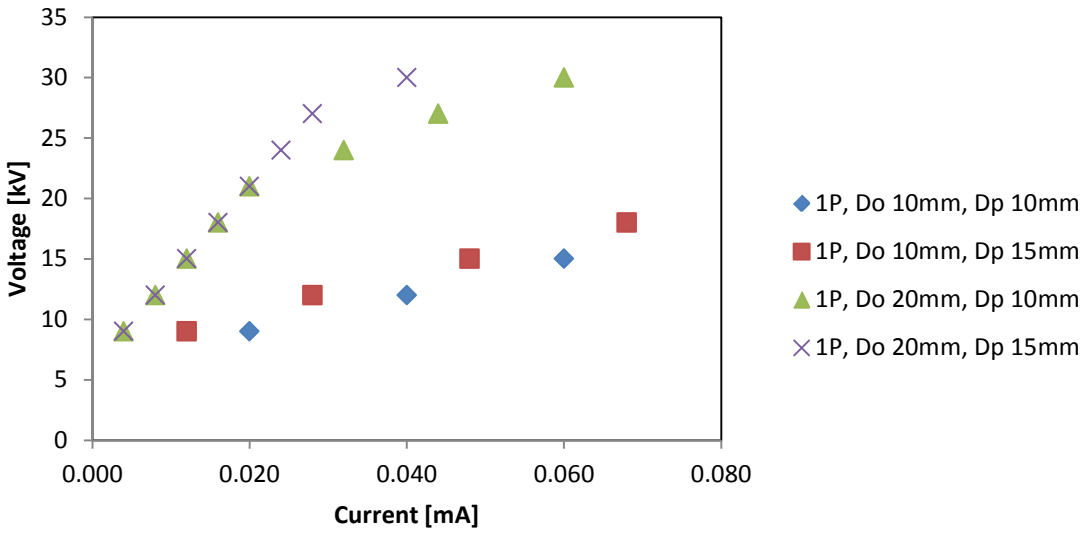

Figure 7: Current voltage characteristics for a single center HV point over oil c

It is important to note that for these tests there existed an air pocket below the ground electrode causing the electrode to tilt slightly. This same issue is prevalent in the 4-point and 19-point tests following in Sections 4.1.1.2 and 4.1.1.3. It is believed that if the ground electrode was perfectly level, a marginally higher current could have been reached before sparking occurred. The violet single point corona discharge is visible in

ambient lighting as shown in Figure 8. Based on the cut of the point tip, there was a tendency for the corona discharge to form two streamers from the point.

Figure 8: Single HV point over oil c with D_o=20 mm and D_p=10 mm

When applied to the gas and liquid oil mediums, the point-to-plane electrode configuration for a corona discharge resulted in the formation of a single conical depression directly below the point. As the voltage was increased, this depression became deeper and wider, eventually sparking directly from the high voltage point to the uncovered grounded electrode. In other words, the liquid oil was displaced so the plasma discharge traveled only through the gas. To create a more uniform surface reducing the depth of the depressions, additional points were added to the high voltage electrode.

4.1.1.2 Four Linear HV Points

Four points at intervals of *s*=2 mm were linearly arranged for the HV electrode as seen in Figure 9. Unlike the single point discharge, these points had a square cross sectional area and the tips were conical.

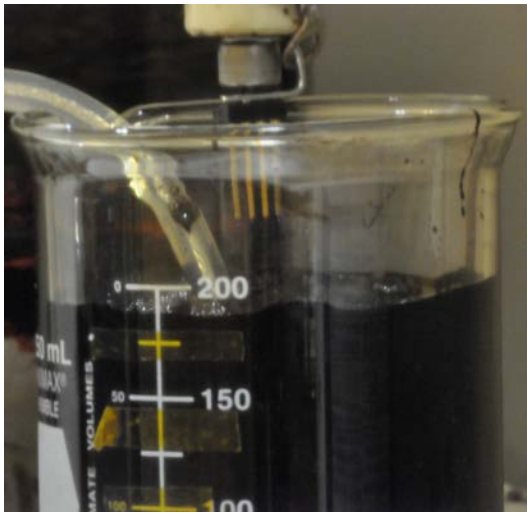

Figure 9: 4-point HV electrode configuration over oil c

When all four HV points exhibited a corona discharge, a rectangular depression formed below the points. However, sometimes a corona discharge was present only on the outer two points, in which case the depression formed was saddle shaped. This is similar to the appearance of the corona discharge on the periphery of the multipoint electrode tested by Jaworek and Krupa [8]. Figure 10 shows the violet corona discharge on the outer points, easily visible only without ambient lighting.

Figure 10: 4-point HV electrode with plasma discharge on outer two points, exposure time 1/15 sec.

The VI trend shown in Figure 11 is similar to that of the single point discharge, with the oil depth having a greater overall effect on the VI characteristics than the distance from the HV points to the surface of the oil. However, for this set up the maximum current of 0.060 mA was obtained at D_o=20 mm and D_p=10 mm. The lower current for the 4-point electrode than the single point electrode was due to the close spacing of the points. This small spacing had an additive effect on the depth of the depression resulting in a deeper depression at lower currents.

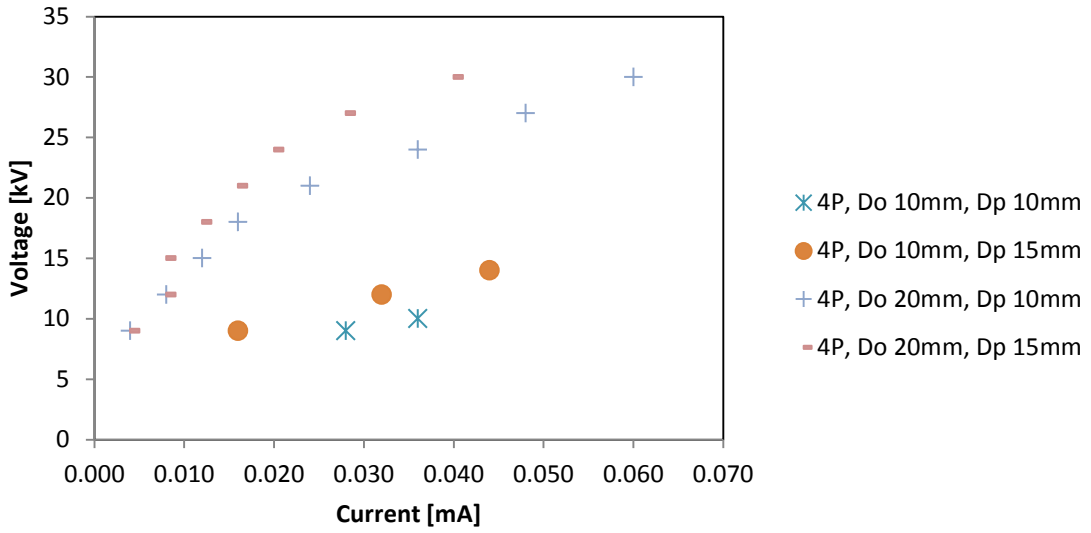

Figure 11: Current voltage characteristics for 4 linear HV points over oil c

4.1.1.3 Nineteen HV Points

It was believed that a hexagonal configuration of points would preserve the uniformity of the surface of the oil for a higher current and voltage (Figure 12) while providing a more uniform treatment of the oil. To this effect 19 points each with a length ℓ =15.6 mm were arranged on a circular steel mesh in a hexagonal pattern at intervals of s=22.23 mm. A larger spacing was used between the points to prevent the additive depth effect observed with the 4-point linear arrangement in Section 4.1.1.2. Each of the points was fabricated as stated in Section 3.1.1 (Figure 3). Note the lower left picture in Figure 12 displays the general electrode set up with a solid piece of metal instead of the mesh for easier visualization.

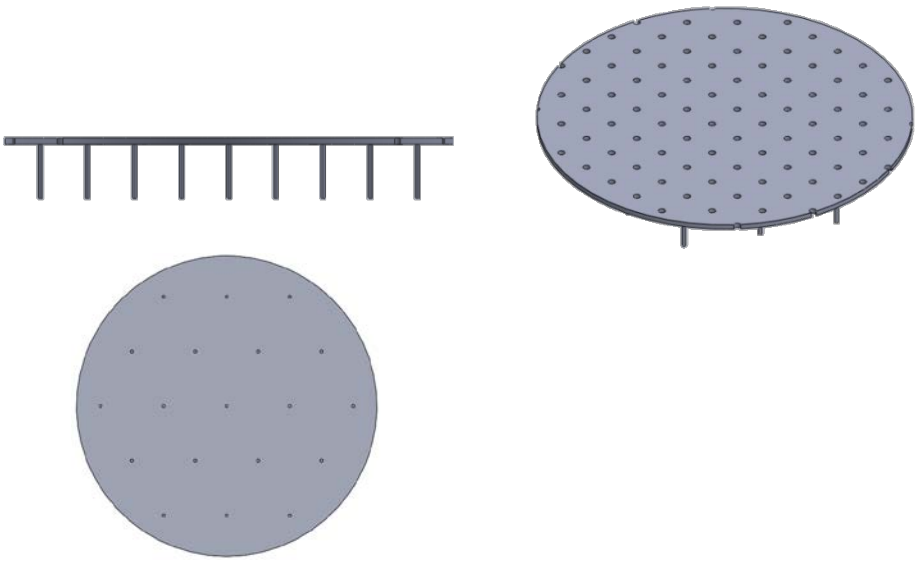

Figure 12: 19-Point high voltage electrode

The violet discharge was easier viewed without ambient lighting as shown in Figure 13. Not all of the HV points exhibited a discharge and those that did, did not all have equal magnitudes due to the angle of the ground electrode created from the air pocket mentioned previously in Section 4.1.1.1. The ground electrode is higher on the right side than the left. Each point resulted in local conical depressions in the oil.

Figure 13: 19-point HV electrode over oil c with D_o=20 mm and D_p=15 mm at V=15 kV and I=0.188 mA, exposure time 1/15 sec.

The VI trend in Figure 14 does not show the results for D_o=10 mm and D_p=10 mm because breakdown of the corona discharge was immediate. Instead it includes an additional measurement at D_o=20 mm and D_p=12 mm. The VI trend is similar to that found with the single and 4-linear HV points. However, the same current can be reached with a much lower voltage input than for either of the two previous HV electrode configurations. The maximum current of 0.364 mA occurred at D_o=10 mm and D_p=15 mm. The VI trend for D_p=12 mm mirrored that of D_p=15 mm until a voltage of 21 kV was reached. At D_o=20 mm and D_p=10 mm the point tips were slightly wetted by the oil.

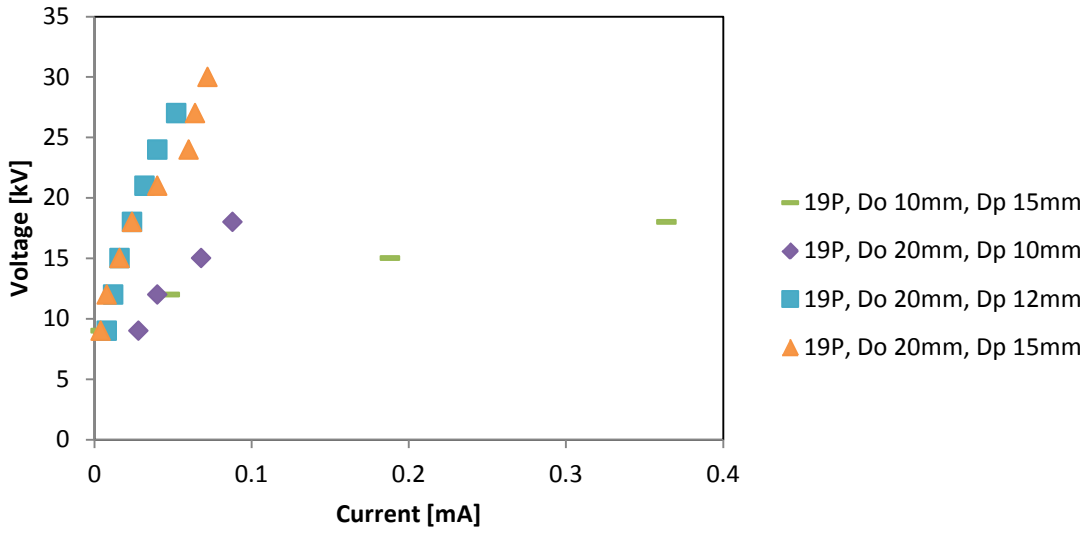

Figure 14: Current voltage characteristics for 19 hexagonal HV points over oil c

4.1.2 Electro-hydrodynamics

For all HV electrodes, observation revealed that there exists an optimum distance between the high voltage points and the surface of the oil. When the distance is too small, the points become wetted with the oil due to the fluctuations (peaks and troughs) of the oil. This phenomenon can be seen in Figure 15. The lowest point of the troughs is directly underneath an HV point and the highest point of the peaks is centered around an HV point. The horizontal line represents the original depth of the oil, i.e. after the oil was heated and before the power supply was turned on, which was kept constant while D_p was varied. The troughs and peaks are conical in shape.

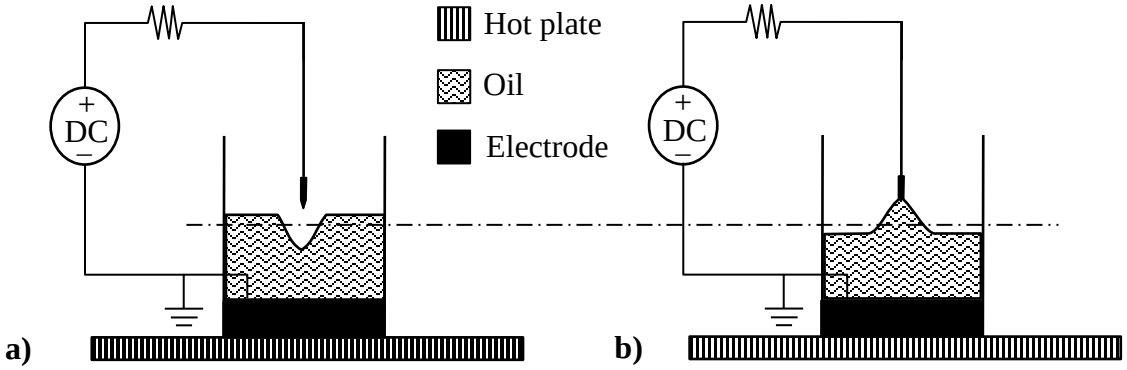

Figure 15: Tendency of surface of oil to form a) troughs and b) peaks directly below a HV point

If the distance between the oil surface and high voltage points is too great, the corona discharge will not form. Between these two extremes, breakdown of the corona discharge to a spark discharge occurs when the troughs in the oil become deep enough for the corona discharge to travel directly from the high voltage points to the ground electrode, bypassing the oil. The point at which this occurs is dependent upon the applied current and voltage; as the current and voltage are increased, the trough becomes wider and deeper. This results in an increase in the height of the oil at a distance *x* from the HV point. The peaks lower the height of the oil at a distance *x* from the HV point. For the multipoint electrode, the gaps between the points are filled with peaks, created as a result of the flow of oil from the troughs.

To explain the peak-trough phenomenon (PTP), it is assumed that the oil has a constant, relatively low conductivity. Once corona onset has been reached, an ionic wind forms in the gas region. The ionic or corona wind is created by the repulsion of the

similarly charged ions and point tip and propagates towards the oil surface. This leads to a localized charge build-up on the surface of the oil. The charged oil then moves towards the ground electrode, resulting in a vortex convection field that is symmetrical around the axis of the HV points and a wavy oil surface [59]. This leads to the formation of the troughs seen within the tests in Section 4.1.1.1-4.1.1.3. The troughs in the oil can also be said to be formed by the ionic wind pressure, ranging from a few to several tens of Pascal, at the surface of the oil. This pressure is greatest directly underneath the HV point and lessens with distance from the center. At voltages lower than the corona onset voltage, there exists a small Coulomb attractive force creating peaks on the surface of the oil centered under the HV points. Furthermore, when $D>D_p$ for the case of multiple HV points, there is no interference between the ionic winds and troughs formed from each individual point [60]. While the PTP phenomenon produces undesirable depressions allowing the breakdown of the corona discharge, it has the added benefit of mixing the oil so all of the oil is treated by the corona discharge and not just the surface.

The creation of the peaks surrounding the HV point at smaller D_p may also be due to the high temperature of the oil. Anything that increases the temperature and motion of liquid molecules interferes with the bonds between them. If the temperature of a liquid is high enough or at a certain critical viscosity, it overcomes the force of cohesion between molecules. When the force of adhesion between a liquid and solid is more than 1.5 times as large as the force of cohesion between the liquid molecules, the liquid is said to wet the solid [61]. Another possibility is that the HV points formed unobserved troughs created from a plasma discharge at the two sides of the 45° tip of the

point. However, this formation would only occur if the sharp edges on the point were still exposed, which did not seem to be the case. In Figure 16 the two arrows indicate the supposed troughs; the point is magnified.

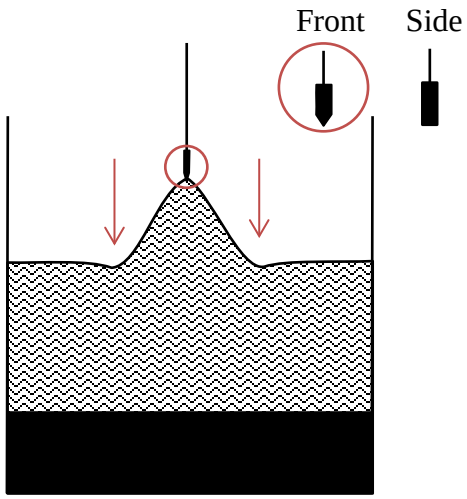

Figure 16: Formation of peak with two small troughs

In terms of the effect of the plasma on the oil, experiments with water have shown that its dielectric characteristics result in localized electric fields and can lead to the formation of a conductive channel and current leaks to the surrounding liquid [11]. The continued application of the electric current induces the local overheating of the corona discharge, which forms weak shockwaves within the liquid [11]. It has also been shown that a pulsed corona operating at 10^2 to 10^3 Hz in water creates relatively weak

shock waves, bubbles, weak to moderate ultraviolet radiation, and radicals and other reactive species in the region near the discharge electrode [18].

4.2 Crude Oil Temperature

4.2.1 Temperature Characteristics of Oil C

The viscosity of the oil is a function of its temperature and is therefore experimentally controlled by varying the temperature of a given crude oil. Oil c was evaluated at a temperature of 100°C (212°F) and 120°C (248°F) for D_o =20 mm and D_p values of 10 mm, 15 mm, and 20 mm. One temperature was evaluated per day. The VI trend is displayed in Figure 17.

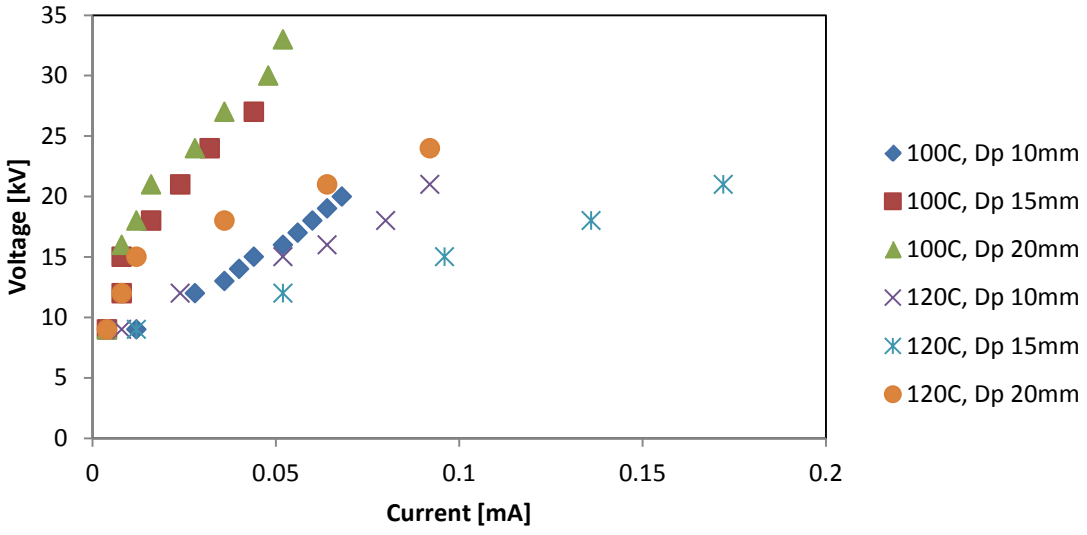

Figure 17: Current voltage characteristics for 19 hexagonal HV points over oil c as a function of temperature

It is believed that the variance of the VI trend for a D_p of 15 mm and 20 mm at 120°C may be attributed to fluctuations in the temperature. When D_p was increased and the temperature of the oil and the oil depth were constant, a higher voltage was necessary to reach the same current at the lower D_p. For a constant D_p and D_o, an increase in temperature lowered the voltage required to reach a certain current. The plasma discharge into the oil created many small bubbles on the surface of oil c (Figure 18). These were still prevalent upon the cooling of oil c to the room temperature of 72°F (22°C) but were no longer apparent when oil c was mixed.

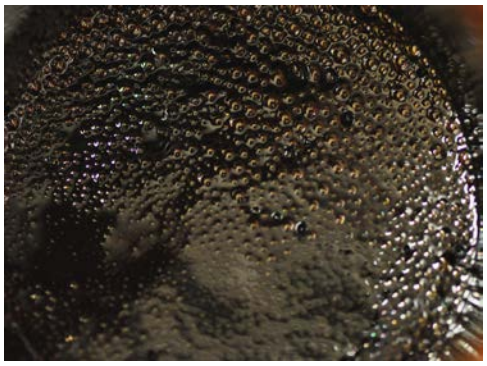

Figure 18: Effects of corona discharge treatment on oil c

4.2.2 Temperature Characteristics of Oil D

Following the same general procedure as the previous experiments, the effect of temperature on oil d was also studied. D_p was set at 15 mm and the oil depth was also set at 15 mm to ensure no wetting of the HV points occurred as seen previously in Section

4.1.1.3 at distances of D_o=10 mm. No air pocket existed below the ground electrode for this test. Four different temperatures were evaluated ranging from 140°C (284°F) to 250°C (482°F). The system was given approximately 30 minutes to reach thermal equilibrium between each run. Due to the nature of the setup, the thermocouple wire was removed during the experiment, so only the initial and the final temperature of the oil were recorded. The first two temperatures had consistent readings. The temperature listed as 210°C, had an initial temperature of 205°C and a final temperature of 216°C. The temperature listed as 246°C had an initial temperature of 250°C and a final temperature of 242°C. These fluctuations in temperature during the test runs account for the variations in the VI trend in Figure 19 that were not seen in previous tests. The two outlying points for 246°C were recorded after the maximum current was reached.

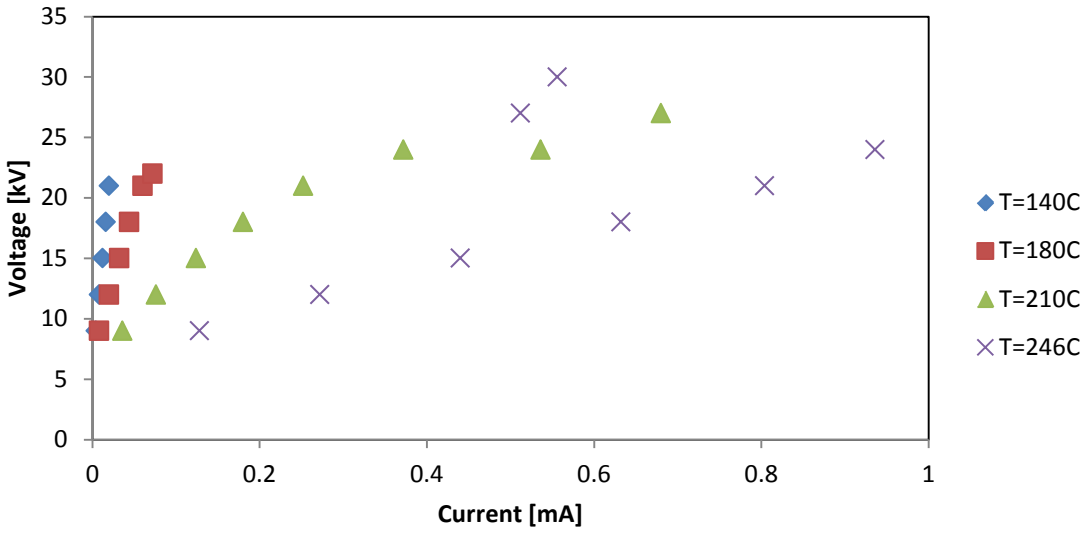

Figure 19: Current voltage characteristics for 19 hexagonal HV points over oil d as a function of temperature

As seen with oil c, a lower voltage was required to reach the same current when the temperature of the oil was higher. The breakdown of the corona discharge to a spark was at significantly higher currents as the temperature increased. It is probable that even higher temperatures than tested would continue to increase the trend. The only limiting factors would be the ignition point of the oil and the temperature limitations of the materials used.

As the voltage and current increased, the strength of the corona streamer or the photons emitted increased. At 24 kV the corona discharge could be seen in ambient lighting, but the full magnitude of the streamers was still better visualized without ambient lighting as shown in Figure 20.

a) 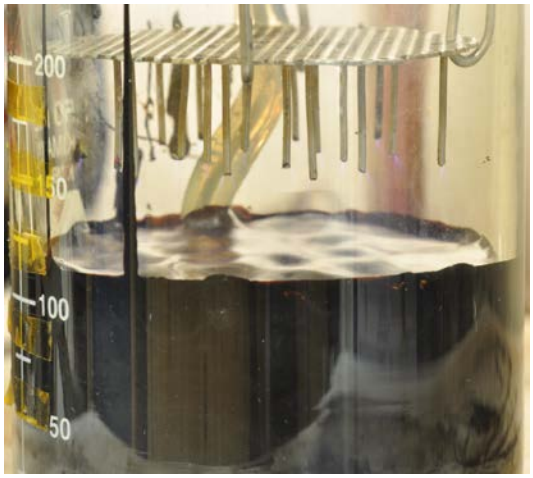

b) 

Figure 20: 19-point HV electrode over oil d for *Do*=15 mm, *Dp*=15 mm, T=210°C, *V*=24 kV, and *I*=0.372-0.536 mA a) with ambient lighting and b) without ambient lighting, exposure time 1.6 sec.

When the voltage was first increased to 24 kV, the current was 0.372 mA. After around 12 minutes, the current had increased to 0.536 mA with no change in the voltage. Breakdown of the HV points from the corona discharge was not simultaneous. At first only a single point would spark at low frequencies around one spark per minute. As the voltage and current were increased past the point of initial breakdown, the frequency and the number of points sparking increased, but all of the points did not spark; some maintained a corona discharge. Similar breakdown characteristics were observed by Kozlov and Solovyov [31]. At the highest temperatures tested, the surface of the oil was nearly flat and did not exhibit high amplitude troughs and peaks underneath the HV points.

4.3 Summary of Preliminary Results

From these preliminary experiments the optimum electrode geometry for the liquid-gas system can be designed. The goal was to have the current at a maximum value and the voltage at a minimum value. The high current enables the greatest amount of dissociation of the hydrogen and the cracking of the heavy hydrocarbon chain of the crude oil. The low voltage ensures that the cumulative energy for the corona discharge treatment time is low enough to create an economically viable process. To achieve this, D_p should be at a minimum, but above the wetting distance, which was 15 mm for all three HV electrodes. It was shown that D_o should also be at a minimum. The highest current was obtained for the 19-point HV electrode. Projection hypothesizes that if more points are added to the hexagonal configuration for the same size mesh, a level oil surface could be maintained longer to reach higher currents. The number of points over the surface area of the oil would however be limited due to the space charge interactions between the points as *s* approaches zero [8]. These results correspond to those achieved in other experiments as described previously in Section 2.3.

5. FINAL EXPERIMENTAL RESULTS

5.1 Distillation Tower

From the preliminary experiments, an electrode and oil configuration was chosen and applied to the corona treatment inside the distillation tower. The HV electrode with 19 points (ℓ =15.6 mm) equally spaced in a hexagonal pattern at intervals of 22.23 mm was used for the distillation tower tests. The aluminum ground electrode had a height of 59.66 mm and a diameter of 16.35 mm. The same HV and ground electrodes were used for all the tests. An extra heavy oil, oil d, covered the ground electrode with a depth D_o = 15 mm above the ground electrode. The distance between the HV points and the surface of the oil was D_p = 15 mm. The following experiments determine the ability of the corona discharge to crack the hydrocarbon chain of an extra heavy crude oil, oil d.

5.1.1 Pure H_2 Gas

Further evaluation of industrial distillation towers revealed that the purpose of the high altitude of the column is to separate the light condensates by their boiling points by way of trays or packing material located periodically along the height of the column [4]. However, the purpose of the distillation tower for this experiment is to separate all the light condensates in a single batch; it is superfluous to separate the different light fractions in the tower. Considering this, the original 85 cm height of the tower (Figure 21) was significantly decreased to 16 cm (Figure 22) and the steel wool packing inside the column was removed. This eliminated the need of the lower heat tape from the original column as well as the variac transformer and temperature probe 16.2 (T_2), thereby increasing the efficiency and precision between tests. All results conducted after

7.18.14 utilized the distillation tower with the shortened column. In Figure 21there is additional insulation that is not shown around the very top of the tower and on the lid of the base chamber.

a)  b) 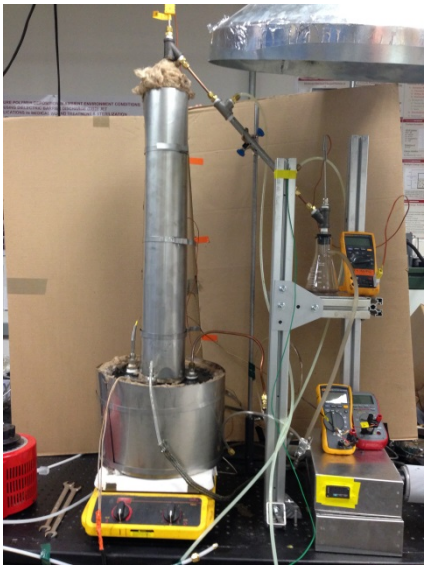

Figure 21: 85 cm tall distillation tower a) without and b) with insulation

a) 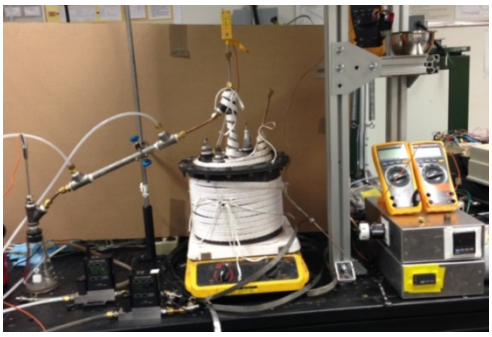 b) 

Figure 22: 16 cm tall distillation tower a) without and b) with insulation

The distillation tower temperature was incrementally increased to the temperatures described in Table 5 in the span of 1.5 to 2 hours. Note the temperatures listed are the averages of the temperature recorded at approximately 30 minute intervals throughout the treatment. The final temperature listed, T_{HP}, is the temperature at which the hot plate was set and is not necessarily the temperature of the bottom of the base chamber (T_5). Tests conducted before 7.3.14 did not monitor the temperature of the bottom of the base chamber. During preheating, hydrogen gas was circulated through the tower at a volumetric flow rate of 2.5 L/min for 45 minutes, whereupon the flow rate was decreased to 0.1 L/min for tests 2.11.14 through 6.25.14 and 0.4 L/min for the remainder of the tests. The higher initial flow rate served to purge the tower of air in order to prevent ignition of the oil and gas.

Table 5: Average temperature for duration of treatment for a gas of pure H_2

Test	VoltCurMon	T_1 [°F]	T_2 [°F]	T_3 [°F]	T_4 [°F]	T_5 [°F]	T_{HP} [°F]
2.11.14[a]	-	450	544.3	373.6	72.0	-	~842
2.14.14[a]	-	450	567.3	387.5	76.0	-	~842
6.4.14[a]	178, 179	450	616.9	449.9	79	-	-
6.25.14[a,b]	207	450	497.5	449.2	83	-	-
7.3.14	208, 209	450	473.4	450.1	81	464.6	374
7.9.14	210, 211	450	540.3	450.0	77.1	468.1	392
7.14.14	-	450	511.4	451.1	81.4	463.2	392
7.15.14	-	601	622.3	601.4	77.1	619.7	527
7.18.14	-	451	531.5	450.6	78.3	462.7	392
7.25.14	-	451	-	450.6	80.2	461.3	392
7.29.14	233, 234	450	-	450.5	87.5	462.1	412
8.1.14	235, 236	475	-	473.4	84.2	483.3	419
8.4.14	237, 238	475	-	469.8	89.9	512.9	473
8.7.14	244, 245	475	-	472.8	88.3	530.4	473
8.12.14	252, 254	480	-	479.7	92.0	511.2	473

[a] $\dot{V}_{H2}$=0.10 L/min
[b] R=4.994 MΩ

The numbers listed under VoltCurMon refer to the LabVIEW recorded voltage and current files. The last VoltCurMon number listed in Table 5 is for the VI trend throughout the 4 hour treatment; preceding numbers are for determination of the maximum current and voltage to use for the treatment. The pivotal temperatures affecting the outcome of the experiments are $T_1 \approx T_3$ and T_5. T_3 is the temperature at which the evaporated oils condensed, or their boiling points. It should be noted that the first two tests did not have equal T_1 and T_3, differing by approximately 70°F.

Breakdown of the corona discharge could not be viewed while the corona reactor was located within the distillation tower. Therefore, following the 2 hours of preheating, a preliminary test lasting between 5 to 30 minutes was conducted to determine the

maximum possible current before sparking occurred because. This was accomplished by gradually increasing the voltage and current on the DC power supply to discover the voltage and current trend of the system. The trend was monitored and recorded by LabVIEW. The first test was an exception in that its VI trends were recorded by hand from a set of multimeters connected to the power supply. The voltage and current characteristics for these pretests can be seen in Figure 23 and Figure 52 in Appendix C.

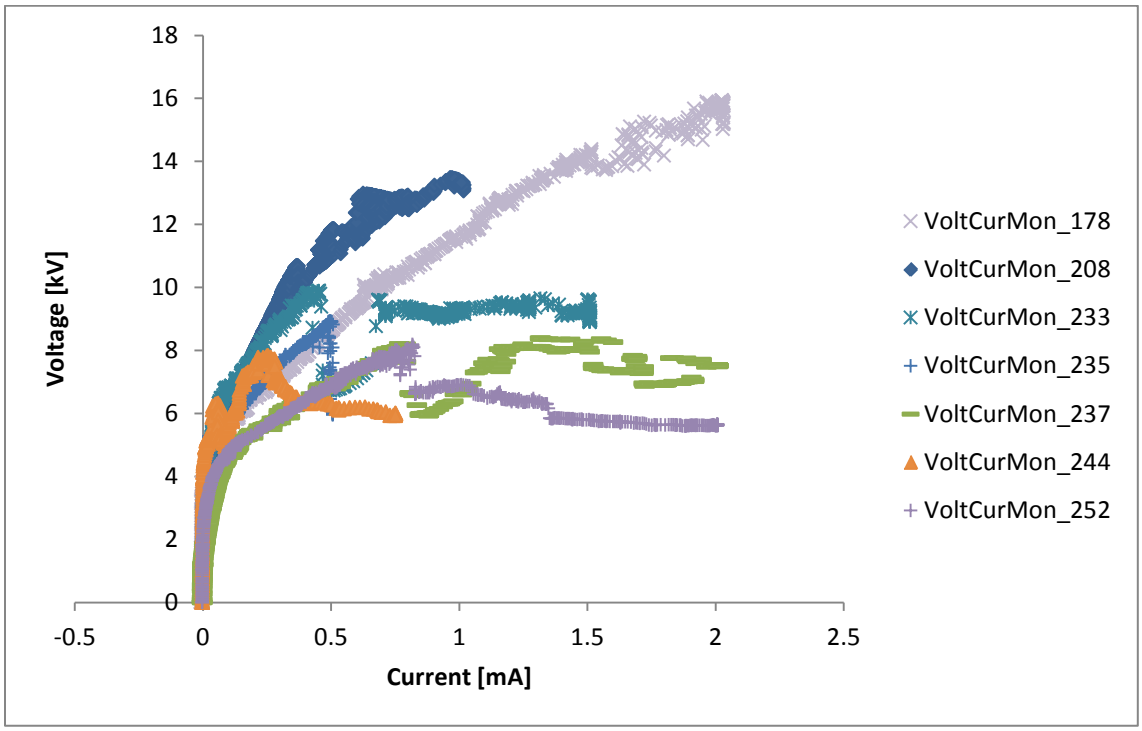

Figure 23: Pretests for determination of voltage and current characteristics for oil d with H_2 in the distillation tower

VoltCurMon_208 and VoltCurMon_233, both at $T_1 \approx T_3$=450°F and with similar T_5, have comparable trends up until sparking occurs around 10 kV. VoltCurMon_175 to VoltCurMon_178, also at T_1=450°F, have a similar trend to the aforementioned two curves and show the precision of the voltage and current measurements for a single test. Although $T_1 \approx T_3$=475°F for VoltCurMon 235, 237, and 244, the temperature of the hot plate was increased for each subsequent run (483.3°F, 512.9°F, and 530.4°F respectively) which lowered the viscosity of oil d and increased its conductivity. This is reflected in the graph by the lower voltage requirements necessary to achieve the same current. VoltCurMon_252 is at T_1=480° and T_5=511.2° and displays a trend parallel to VoltCurMon_237. It should be noted that VoltCurMon_178 had the smoothest trend with no obvious point of breakdown.

On 8.12.14 multiple pretests were taken evaluating the effect of only T_1 on the conductivity of the oil. The temperatures for the system are listed in Table 6. T_{HP} was kept constant at 473°F, however T_5 fluctuated slightly from 512.1°F, 510.0°F, 507.1°F, and 505.6°F for VoltCurMon 250, 251, 252, and 253 respectively. The VI trends for these preliminary tests are shown in Figure 24.

Table 6: Average temperature for preliminary tests on 8.12.14 with pure H_2

Test	VoltCurMon	T_1 [°F]	T_2 [°F]	T_3 [°F]	T_4 [°F]	T_5 [°F]	T_{HP} [°F]
8.12.14[a]	250	491	-	494.5	93.7	512.1	473
	251	484	-	476.8	93.9	510.0	473
	252	479	-	480.7	93.0	507.1	473
	253	474	-	477.8	92.8	505.6	473

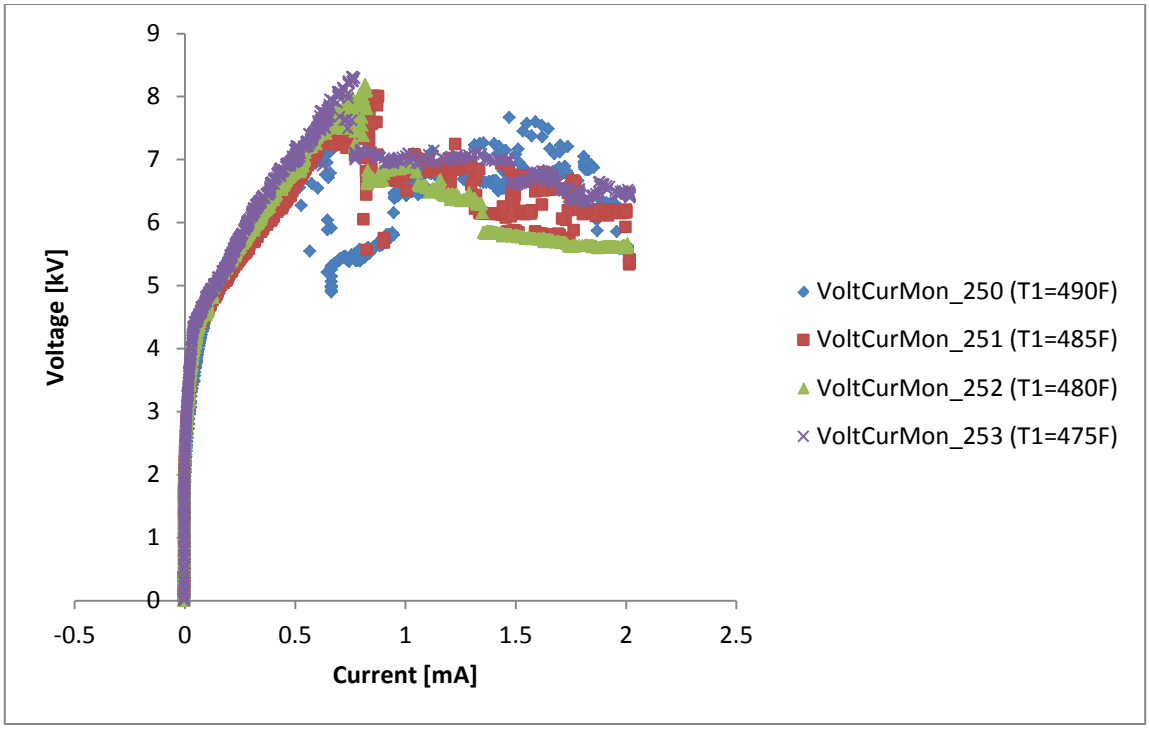

Figure 24: Evaluation of T_1 effect on VI trend for oil d with H_2 in the distillation tower

In general, a marginally higher voltage was needed to maintain the same current as the temperature T_1 decreased. Sparking occurred at a lower current when T_1=490°F than for the other temperatures. The highest current was achieved at 480°F, closely followed by 475°F. The drop in current at the two highest temperatures resulted from the temperature limitations of the internal electrical wire insulation materials; therefore the maximum temperature that the distillation tower should be operated at is 480°F. Based on these results and those displayed in Figure 23, it can be seen that the temperature setting of the hot plate has the greatest effect on the temperature and therefore the conductivity of the

oil. This is partially due to the flow rate decreasing the amount of time the incoming gas preheats in the tubing before entering the base chamber.

In general, breakdown of a corona discharge to a spark discharge is signified by a drop in the voltage and the power supply becomes current limited. However, for a multipoint discharge not all the HV points breakdown simultaneously and a major drop in voltage may not be seen. A corona discharge is also characterized by a steady stream of light from the HV points to the surface of the oil and is accompanied by a constant hissing noise due to the change in gas pressure at the point tip. When a spark occurs, there is a cracking sound as a bolt of light travels between the HV points and ground electrode. Although the plasma discharge was not audible or visible within the distillation tower, it was determined that sparking occurred when the power supply continuously switched between being current and voltage limited. This was seen real-time in LabVIEW as a sudden spike in current and a sudden drop in voltage. The current and voltage immediately prior to this point were determined to be the maximum for the corona discharge. Generally, this occurred when $V_i - V_{i+1} \geq 0.2\ kV$. These maximum values, tabulated in Table 7, were then used for the treatment of the oil. The voltage recorded is the discharge voltage and takes into account the ballast resistor.

Table 7: Distillation tower treatment current and voltage

Test	VoltCurMon	Maximum Current [mA]	Maximum Voltage [kV]	Cumulative Energy [kJ]	Total Time [min]
2.11.14	-	0.76	10.06	97	210
6.4.14	175	0.48	9.76	7.5617	8.7
	176	0.77	10.83	3.9714	7.2
	177	0.86	10.87	4.7193	7.5
	178	0.69	10.35	4.2697	6.6
	179	0.68	10.36	19.2738	113.2
6.25.14	207	0.57	9.81	85.0325	244.6
7.3.14	208	0.37	10.68	8.1757	27.6
	209	0.54	11.94	92.0987	240.9
7.9.14[a]	210	0.86	11.12	7.8968	20.6
	211	0.66	10.30	8.7382	36.9
7.29.14	233	0.45	9.89	1.7940	6.6
	234	0.40	9.06	37.2318	227.2
8.1.14	235	0.46	8.09	0.5944	5.8
	236	0.42	8.45	40.6624	237.1
8.4.14	237	0.79	8.19	2.6050	8.5
	238	0.79	8.11	69.7594	246.8
8.7.14	242	0.29	6.31	0.9371	4.3
	244	0.35	6.82	1.8264	7.2
	245	0.31	6.54	19.3989	239.5
8.12.14	250	0.52	6.93	2.5107	10.2
	251	0.63	7.43	2.4218	9.0
	252	0.69	7.80	2.4144	10.5
	253	0.64	7.73	2.1035	8.8
	254	0.76	7.95	80.1669	247.2

[a] Control run

The heavy oil was then treated for 4 hours (3.5 hours for the first two tests) with the corona discharge. The current and voltage fluctuations during this time were recorded in LabVIEW (see Appendix B for details). The VI characteristics are shown in Figure 25. At the end of the 4 hours, the power supply, heaters, and recirculator were turned off and the distillation tower cooled overnight. Although not monitored, it is

possible that the HV points eroded to some degree over time as the experiment progressed (same HV electrode used throughout).

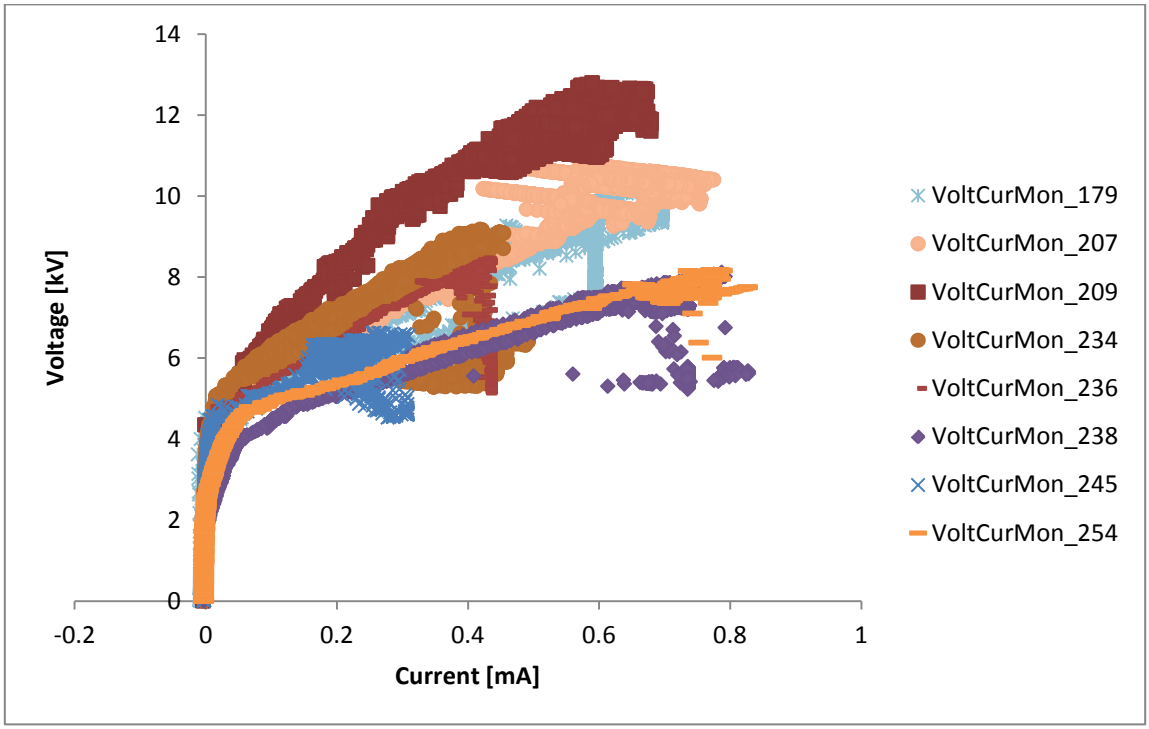

Figure 25: Current and voltage characteristics during 4 hour corona treatment of oil d with H_2 in the distillation tower

As can be seen in Figure 25, the voltage at first exponentially increased until the corona onset voltage was reached. After the corona onset voltage, many of the tests displayed a near-linear relationship between the voltage and the current until breakdown to a spark discharge. Similar trends were observed for each 4-hour test as compared to its pretest. However, as the gas and the oil became ionized, there was an increase in the

current by several tens of microamps before it leveled out. As time progressed and the oil evaporated reducing the liquid oil level in B_1, the current decreased while the voltage remained constant (see Appendix B graphs).

For the 85 cm column an additional step was taken to ensure that any condensate entrained within the base chamber and column condensed into B_2. The day following the corona treatment, B_1 was extracted from the base chamber and the tower was again heated to the desired temperature of $T_1 \approx T_3 = 450°F$ in the span of 2 hours. This temperature was kept constant for 3 hours before the heaters were turned off.

In addition to the plasma treated tests, control tests were executed to determine whether the formation of condensates from the extra heavy crude oil was due to the corona discharge, the heating of the distillation tower, or some combination thereof. The only difference between the control experimental procedure and the corona treated oil procedure was the presence of the corona discharge itself; both were heated to the same temperature for the same amount of time and had the same hydrogen volumetric flow rate.

The mass, measured with an Ohaus Scout Pro SP2001 mass scale, and the volume of the residuals in B_1 and the condensates in B_2 were recorded and the density was calculated. The mass scale had an accuracy of 0.1 g and the volume uncertainty was 0.2 mL. The condensate masses were weighed while still in B_2 and the weight of B_2 was subtracted. This resulted in a calculated uncertainty of 0.2 g for all condensate masses listed in Table 9. The uncertainty for the residual mass is ±0.2 g. At a temperature of $T_3 = 450°F$, all of the control tests yielded a condensate mass within the uncertainty. Any

condensate that formed was not present in B_2 until the following morning after the 7 hour treatment the preceding day. With the increase of temperature to $T_1 \approx T_3$=600°F, a significant amount of condensate, 1.1 g, was formed (Figure 26).

Figure 26: Condensate (left) and corona residue (right) produced from control test 7.15.14 at 600°F $\dot{V}_{H2}$=0.40 L/min

The density of the condensate was originally calculated as 875.0±32.5 kg/m^3. With the removal of B_1 and reheating of the distillation tower, more condensate exited into B_2 yielding a new density of 1125.0±376.3 kg/m^3. For test 7.3.14, there is a discrepancy between the initial mass, recorded on a different day, and the residual mass. It is believed this is due to inconsistencies in the calibration of the mass scale. The 70°F temperature difference between T_1 and T_5 of tests 2.11.14 and 2.14.14 meant that a significant portion of the condensate remained within the distillation tower and did not

collect in B_2. For test 2.11.14 the initial mass of oil d was not measured; instead the initial volume was calculated from the height of the oil and inner diameter of the beaker (68 mm). These values are displayed below in Table 8.

Table 8: Volume of oil d for corona discharge in distillation test 2.11.14

	D_o [mm]	Volume [mL]
Initial	15	55
After treatment	13	46

The percent mass reduction in B_1 from the initial mass to the final mass was calculated by Equation (8).

$$\%\, reduction\ in\ B_1 = \frac{m_{initial} - m_{residual}}{m_{initial}} \times 100\% \tag{8}$$

Similarly, the percentage of oil that was converted to condensate was determined by Equation (9).

$$\%\, conversion\ to\ condensate = \frac{m_{condensate}}{m_{initial}} \times 100\% \tag{9}$$

Table 9: Mass and density of condensates formed during treatment in the distillation tower

	Test	$T_1 \approx T_3$ [°F]	T_5 [°F]	Cumulative Energy [kJ]	Initial Mass [g]	Residual Mass [g]	% Mass Reduction in B_1	Condensate Mass [g]	% Conversion to Condensate	Condensate Density [kg/m^3]
Corona Treated	2.11.14[a,b]	450/375	-	97	-	51.0	-	2.1	-	640.0±64.2
	6.4.14[a,b,c]	450	-	19.2738	52.1 ± 0.1	44.2	15.2	1.9	3.6	653.8±63.3
	7.3.14[a]	450	464.6	92.0987	51.0 ± 0.1	51.9	-	0.4	0.8	-
	7.29.14	450	462.1	37.2318	52.4 ± 0.2	52.3	0.2	< 0.1	0.1	-
	8.1.14	475	483.3	40.6624	52.3 ± 0.2	52.1	0.4	< 0.1	0.1	-
	8.4.14	475	512.9	69.7594	51.1 ± 0.1	50.9	0.4	0.1	0.2	-
	8.7.14	475	530.4	19.3989	51.7 ± 0.1	51.5	0.4	0.2	0.4	-
	8.12.14	480	511.2	80.1669	52.0 ± 0.1	51.8	0.4	< 0.1	0.1	-
Corona +Heat Treated	6.25.14[a,b]	450	-	85.0325	51.9 ± 0.1	20.9	59.7	16.7	32.2	878.0±32.5
Control	2.14.14[a,b]	450	-	-	34.5 ± 0.1	33.9	1.7	0.4	1.2	-
	7.9.14[a]	450	468.1	-	51.0 ± 0.2	51.0	0	< 0.1	0.1	-
	7.14.14[a]	450	463.2	-	51.9 ± 0.1	51.9	0	< 0.1	0.1	-
	7.15.14[a]	600	619.7	-	51.9 ± 0.2	51.3[d]	1.2	1.1	2.1	875.0±251.9
	7.18.14[a]	450	462.7	-	51.4 ± 0.3	51.3[d]	0.2	0.2	0.4	-
	7.25.14	450	461.3	-	51.3 ± 0.3	51.3[d]	0	0	0	-

[a] 85 cm distillation tower. The remaining experiments were conducted in the 16 cm tower.

[b] $\dot{V}_{H2}$=0.10 L/min. The other experiments were conducted at 0.40 L/min.

[c] R=4.994 MΩ

[d] Residual mass uncertainty ± 0.3 g

As can be seen in Table 9, the corona treated oil overall yielded more condensate than the thermal treatments, but the condensate was still within the mass uncertainty. Test 7.3.14 had the highest cumulative energy input of 92.0987 kJ as a result of the relatively lower temperature ($T_1 \approx T_3$=450°F and T_5=464.6°F) of the system limiting the conductivity of the oil. The extremely large condensate production for test 6.25.14 may be attributed to an additional thermal treatment. Following the standard 4 hour corona treatment, everything (heaters, recirculator, gas flow, power supply) except the hot plate was turned off. The hot plate was left at maximum ($\sim T_{HP}$=842°F) for 18 hours, then a 4 hour thermal treatment of oil d at was conducted. The combination of corona and thermal treatment resulted in a powdery coke residue as shown in Figure 27 and a residue with a density of 878.0±32.5 kg/m^3. This was a stark contrast to the moist residue normally remaining in B_1 from the corona treatment (Figure 28) and signifies that more condensate could have been produced from all of the corona residues.

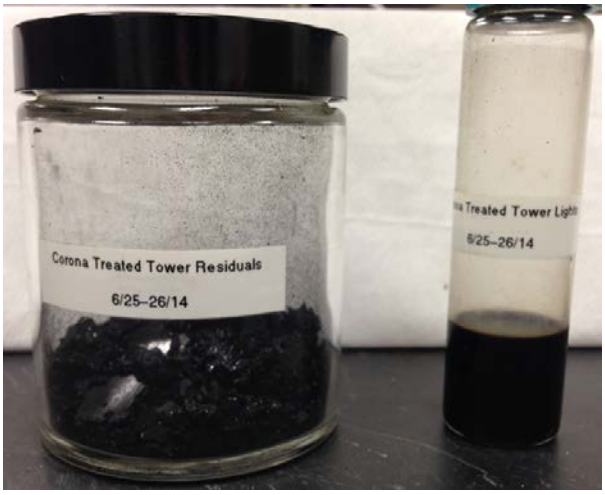

Figure 27: Corona and thermally treated test 6.25.14 carbon residue (left) and condensate (right)

Figure 28: Corona treated test 6.4.14 corona residue (left) and condensate (right)

Tests prior to 6.25.14 yielded a greater amount of condensate than those after 6.25.14. However, the temperature of the hot plate was not monitored with T_5 and instead solely relied upon the temperature display of the hot plate. In addition, at that

time, the hot plate was at a temperature of around 752-842°F during the corona treatment of test 2.11.14 and 2.14.14. Other research has shown that a temperature exceeding 660°F (349°C) [4] or 410°C (770°F) [42] results in the thermal cracking of crude oil. Therefore, while the corona discharge did produce lighter hydrocarbons (2.1 g for test 2.11.14), a portion of that must be attributed to thermal cracking (control test 2.14.14 produced 0.4 g of condensate). See Figure 29 and Figure 30 for pictures of the residue and condensate for these two tests.

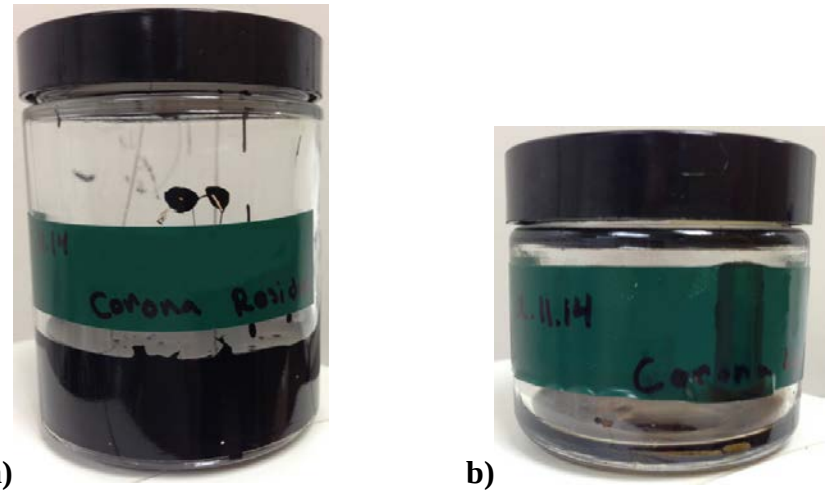

a) **b)**

Figure 29: Corona treated test 2.11.14 at $\dot{V}_{H2}$=0.10 L/min and $T_1 \neq T_3$ a) corona residue and b) condensate

Figure 30: Residue (left) and condensate (right) for control test 2.14.14 at $\dot{V}_{H2}$=0.10 L/min and $T_1 \neq T_3$

For the corona treated oil, the condensate that was collected in B_2 did not fully account for the change in mass of the original oil in B_1. It is possible that some of this oil remained inside the distillation tower. For the tests on 8.4.12 and 8.12.14, when B_1 was extracted from the base chamber, it was coated with dried condensate as shown in Figure 31. Several of the tests also exhibited moist condensate on the inside of the 1000 mL beaker and the petri dish.

a) 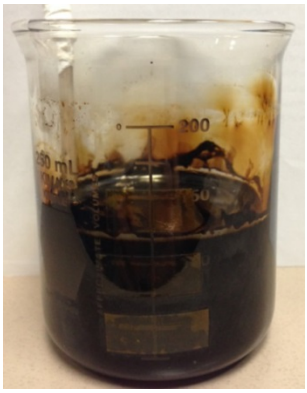 b) 

Figure 31: Dried oil d condensate coating on inside of B_1 for test on a) 8.4.14 and b) 8.12.14

Analysis of the condensate produced the following mass spectrometry in Figure 32, courtesy of the Texas A&M University Laboratory for Biological Mass Spectrometry (TAMU/LBMS). A Matrix-Assisted Laser Desorption Ionization Mass Spectroscopy (MALDI-MS) analyzed the condensates. The base peak (bp) of the condensate was 244.0 m/z with an atomic mass of 2255 AMU. More detailed results of the analysis are displayed in Appendix D.

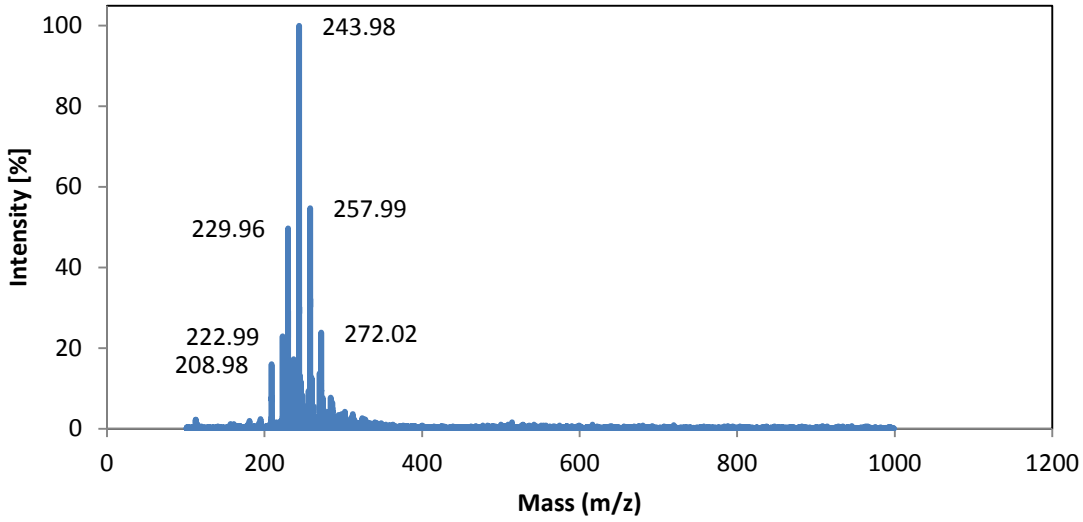

Figure 32: Mass spectrometry of condensate collected on 4.29.14[1]

The majority of the molecules have a mass-to-charge ratio within the range of 177 to 372 m/z.

In industry, extra heavy oils are often processed through delayed coking. The range of condensate products varies depending on the original feedstock but can include alkanes, alkenes, naphtha, and gas oil [4]. Various alkanes and alkenes with boiling points below T_3 are listed in Table 10. It is possible that one or more of these molecules was present in the condensate collected in B_2. In terms of marketable products, the condensate is most likely petroleum diesel, which has a boiling point ranging from 350°F to 700°F [4] and can contain 8 to 21 carbon atoms per molecule with a density of 832 kg/m^3.

[1] Use of the TAMU/LBMS is acknowledged.

Table 10: Possible molecules for condensate formed from oil d [22]

Molecule		AMU	Boiling Point [°F]	Density [kg/m^3]
Alkane	C_5H_{12}	72.146	97	626
	C_6H_{14}	86.172	154	659
	C_8H_{18}	114.22	211	692
	$C_{10}H_{22}$	142.28	345	730
	$C_{11}H_{24}$	156.3	385	740
	$C_{12}H_{26}$	170.33	421	750
Alkene	C_5H_{10}	70.13	86	641
	C_6H_{12}	84.156	146	673
	C_8H_{16}	112.21	250	710 [a]
	$C_{10}H_{20}$	140.26	339	740 [a]
	$C_{12}H_{24}$	168.31	416	758

[a] Value obtained from MSDS for respective molecule

Assuming an energy charge of $0.11/kW-hr based on the utility rates in the area, the energy requirements to produce the condensate are as follows in Table 11. For condensate masses less than 0.1 g, it is estimated that their mass is 0.05 g. The energy cost per barrel of oil is calculated from the densities listed in Table 9. For those without listed densities, the average density of 809.4 kg/m^3 is assumed. This is equivalent to an API gravity of 43.3°. The energy costs calculated take into account the cumulative energy recorded for the corona discharge but not the energy required to heat the distillation tower, the energy required to operate all the equipment, nor the cost of

hydrogen. The first four columns in Table 11 are in terms of the condensate produced and the last two columns are based on the initial untreated mass of oil d.

Table 11: Energy requirements for condensate mass produced from corona treatment of oil d

Test	% Conversion to Condensate	Condensate Specific Energy [MJ/kg]	Energy Cost [$/kg]	Energy Cost [$/bbl.]	Initial Mass Specific Energy [MJ/kg]	Energy Cost for Initial Mass [$/bbl.]
2.11.14	-	46.2	1.41	143.61	-	-
6.4.14	3.6	10.1	0.31	32.22	0.37	1.18
6.25.14	32.2	5.1	0.16	21.72	1.64	6.99
7.3.14	0.8	230.2	7.04	1118.53	1.81	8.77
7.29.14	0.1	744.6	22.75	3118.14[a]	0.71	2.79
8.1.14	0.1	813.2	24.85	3405.45[a]	0.78	3.06
8.4.14	0.2	697.6	21.32	2921.15[a]	1.37	5.37
8.7.14	0.4	97.0	2.96	406.16[a]	0.38	1.48
8.12.14	0.1	1603.3	48.99	6713.92[a]	1.54	6.06

[a] Based on average density of 809.4 kg/m^3

Considering all of the tests, including those with a questionable additional thermal treatment (the first three tests), the lowest costs were for test 6.25.14 at $21.72/bbl. of condensate and test 6.4.14 at $1.18/bbl. of untreated oil d. The average cost of the corona treatment was $4.46/bbl. of untreated oil d. For 2014 (Jan. – Aug.) the average refiner acquisition cost of crude oil was $99.04/bbl. [62]. The cost for refining is the difference between the monthly average of the price of diesel and the crude oil purchase price and typically accounts for 13% of the retail price [63]. Refining costs

$20.97/bbl. based on the current average retail price of $3.84/gallon of diesel [63]. Other data suggests current industrial refining processes typically cost from $2.20/bbl. to $5.59/bbl., which is on par to the lowest cost attained with this corona reactor [64]. However, this is not specific to the cost to upgrade heavy crude oils, which would have larger expenditures due to the additional equipment and refining processes involved. In 2009, the operating cost for atmospheric residue was $1.1/bbl. for delayed coking, $3.7 to $5.0/bbl. for integrated combined cycle power generation plants, and $2.4 to $2.7/bbl. for a residue fluid catalytic cracking unit [65]. For the processing of Arabian heavy oil, the operating cost ranges from $6.6/bbl. to $8.85/bbl. depending on the cracking technique [65]. Therefore, currently the corona reactor is still on the expensive side, but it has economic potential.

5.1.2 Gas Combination of H_2 and CH_4

Due to the large availability of methane or natural gas in the oil industry, the effects of a combination of methane and hydrogen gas inside the distillation tower were evaluated. For this test, the ballast resistor was 4.994 MΩ. The 85 cm tower was preheated for 1.5 hours and the average temperatures throughout the duration of the test are listed in Table 12. The volumetric flow rate to purge the air from the tower was $\dot{V}_{H2}$=1.88 L/min and $\dot{V}_{CH4}$=0.62 L/min. After 45 minutes, the flow rates were lowered to $\dot{V}_{H2}$=0.1 L/min and $\dot{V}_{CH4}$=0.03 L/min. There was no pretest and the total corona treatment time was 5 hours after which all heaters and the recirculating system were turned off and the tower cooled overnight

Table 12: Average temperature for duration of treatment of oil d with a gas combination of H_2 and CH_4

Test	VoltCurMon	T_1 [°F]	T_2 [°F]	T_3 [°F]	T_4 [°F]	T_5 [°F]	T_{HP} [°F]
5.21.14	155	450	557.4	450.2	79	-	455

Halfway through the corona treatment the power supply was turned off for 15 minutes and a 1 kΩ resister was added to the circuit between the ground electrode and grounding strap to check for possible current leaks. This resulted in a sudden drop in the VI (see Appendix B, Figure 50 and Figure 51). The new resister revealed that there was a current leak present in the system; therefore the current and voltage on the power supply were adjusted to account for this for the remaining 2.5 hours. The overall VI characteristics are displayed in Figure 49.

The cumulative energy for this test was 316.1377 kJ over a time period of 292.3 minutes. No oil condensed into B_2, but there was condensate present on the inside of B_1, the petri dish, and the 1000 mL beaker shown in Figure 33. The location of the condensate was partially attributed to the lack of insulation on the lid of the base chamber. In subsequent tests (after 5.25.14), additional insulation covered the lid. The crystalline formation of condensate on the 1000 mL beaker is located where the HV and ground wires entered into B_1. The corona cracking of oil d reduced the mass of the residual oil in B_1 from 50.0 ± 0.1 g to 49.3 ± 0.2 g (includes the mass of the condensate on the walls of B_1).

a)

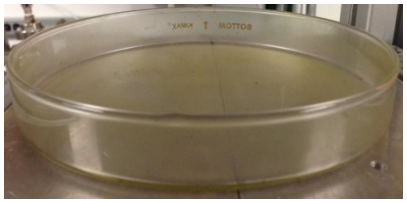

b)

c)

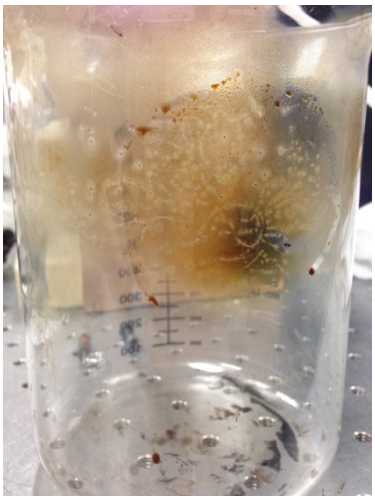

Figure 33: Test with H_2 and CH_4 oil d condensate located on a) petri dish, b) B_1, and c) 1000 mL beaker

The most significant result from this test was the formation of carbon fibers on the tips of several of the HV electrode points due to the presence of carbon in the methane (Figure 34). It is probable that these fibers altered the VI trend by changing the gap distance and contributed to the dissipation of the current in the circuit and premature breakdown of the corona discharge.

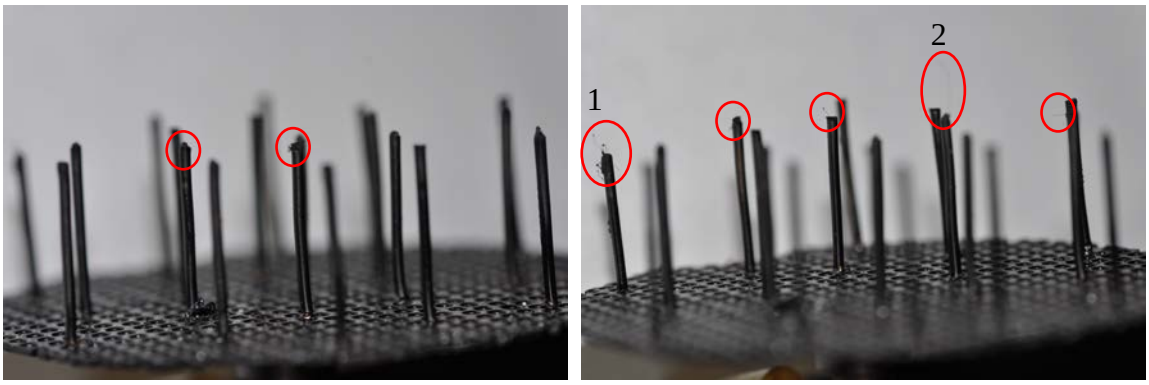

Figure 34: Formation of carbon fibers on HV point tips due to presence of methane gas (varying camera focus)

The largest amount of carbon fibers appeared on points 1 and 2, which are magnified in Figure 35.The dimensions of the fibers were approximated by comparing the number of pixels to the known wire point diameter of 1.024 mm. The two longest fibers on points 1 and 2 had lengths of 2.1 mm and 7.4 mm and diameters of 70 μm and 230 μm respectively.

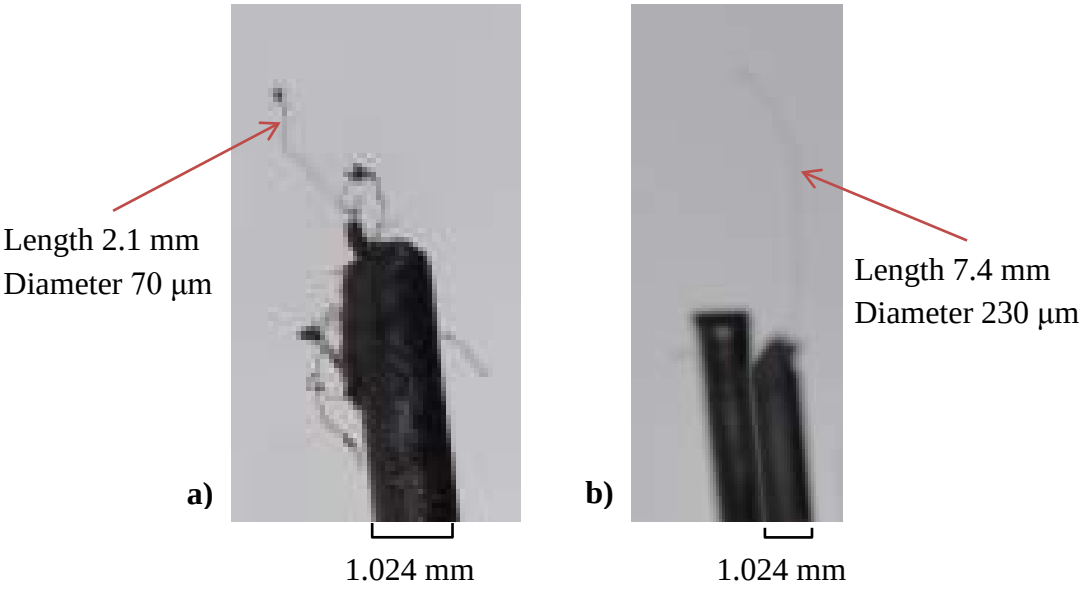

Figure 35: Magnified photos of the carbon fibers on the HV point tips of a) point 1 and b) point 2

Methane was not used in any subsequent tests as one of the sources of hydrogen for the corona cracking of oil d because of the formation of these carbon fibers and their subsequent effect on the electrical circuit of the corona reactor.

6. CONCLUSIONS AND FUTURE WORK

6.1 Summary

The goal of this thesis was to assess the ability of a corona discharge to treat heavy crude oil. To this effect, a corona discharge reactor was created by analyzing the effects of different high voltage electrode geometries based on the conventional point-to-plane configuration in terms of the maximum current achievable. The variables focused upon were the number of high voltage points, the distance between the electrodes, and the depth of the oil. The effect of the temperature of the oil was also analyzed. These first experiments were performed in air at room temperature and pressure. The results of these tests were compared to experiments with similar corona geometries.

For the actual treatment of the oil, a distillation tower was designed to house the corona reactor. The tower was heated to the desired temperatures in a span of 1.5 to 2 hours. The voltage and current characteristics were recorded to verify the maximum current allowed before sparking occurred. This maximum current was then used to treat the heavy oil for 4 hours. The volumetric flow rate of the hydrogen flowing into the tower was 0.4 L/min. The light oil evaporated from the heavy oil and condensed into a beaker located outside of the distillation tower. The masses of the condensate and the oil residue were measured and compared to determine the ability of the corona to crack the long hydrocarbon chains.

6.2 Major Findings

The distance of the HV points from the surface of the oil yielded either a wetting of the points for too close a distance or the formation of a trough directly underneath the points for any distance exceeding the critical distance. Multiple points arranged in a hexagonal pattern leveled the surface of the oil so a larger current could be achieved before the trough deepened, which inadvertently allowed the plasma to spark directly from the HV electrode to the ground electrode. In addition, the multipoint arrangement distributed the charge across the oil and stirred the oil, thereby treating it more evenly. For all HV electrode geometries D_o had a greater overall effect on the VI characteristics than D_p. For the corona reactor, the best results occurred when both of these values were at a minimum. An elevated temperature lowered the viscosity of the heavy oil while increasing its conductivity and the maximum current that could be achieved before sparking occurred.

When positioned inside the distillation tower, the light condensates produced from the corona discharge were separated from the heavy residue. The maximum temperature for this process was 480°F. The corona treatment current and voltage were determined by the maximum values achieved before breakdown, which generally occurred when $V_i - V_{i+1} \geq 0.2\ kV$. The change in mass of oil d in B_1 was greater than when the oil was only thermally treated. However, the condensates collected in B_2 were often within the mass uncertainty and did not fully account for the change in mass of B_1. When a 70/30 ratio of hydrogen to methane gas flowed through the distillation tower, carbon fibers formed on the tips of the high voltage points.

6.3 Conclusion

The hydrogen enriched corona reactor is able to crack long hydrocarbon chains. Its efficiency is dependent on the number and geometry of HV points, which affect the formation of troughs within the oil and therefore the maximum current that can be reached before breakdown occurs. A thin layer of oil is desirable. Elevated oil temperatures lower the viscosity and increase the conductivity of the oil, in turn increasing the maximum current. The average energy cost to produce the condensate with the corona reactor is $4.46/bbl. of untreated oil and as such is not yet economical. Several recommendations with the goal of further increasing the efficiency of the hydrocarbon cracking process are described in the following section.

6.4 Recommended Future Work

It is recommended that the corona reactor be up-scaled to treat a larger amount of oil at once. This would increase the amount of condensate produced yielding a mass larger than the uncertainty and more verifiable results. Additionally, it has been shown that a continuous corona discharge is limited by low currents and low power [66]. By pulsing the corona discharge, it is possible to achieve a higher current and power without the formation of a spark due to the generation of electrons without significant motion of the ions [9, 66]. This also has the potential of lowering the treatment time of the oil, but it could negatively impact the temperature during the experiment. After the corona reactor configuration is altered to treat a larger amount of oil, different types of heavy and even medium crude oils should be tested. This would ensure that the corona reactor has an effect on the oils despite compositional differences.

The function of the distillation tower was to separate the light oil fractions from the heavy residue. Often times, the condensates were entrained within the system and did not collect inside the condensate receptacle. It is therefore recommended that the distillation tower configuration and temperature be further optimized. Specifically, one variable that was not entirely addressed was the volumetric flow rate of the incoming gas. It was believed that a lower flow rate was preferable to ensure that the temperature inside the distillation tower remained fairly consistent and that the gas had a long enough residence time to become ionized. It is possible that either the chosen flow rate was still too high or it was too low and did not provide enough hydrogen atoms to crack the long hydrocarbon chains of the oil. One method of analyzing this would be to quantify the ratio of carbon to hydrogen within the residue, condensates, and gas. If relatively high concentrations of hydrogen are present at the gas exit of the distillation tower, a cyclical system should be developed to reuse the gas. This would aid in lowering the overall amount of hydrogen used in conjunction with the corona reactor and therefore the hydrogen gas cost. The ability of the corona discharge to directly lower the overall viscosity of the heavy oil in the presence of a hydrogen gas donor should also be quantified. Comparisons of the untreated oil viscosity with the residue oil viscosity would determine whether the corona reactor cracks a greater amount of oil than what actually condenses at T_3 into the beaker outside of the distillation tower.

Some work has already been accomplished towards treatment of a larger amount of oil by the creation of a 31-point HV electrode to be used in a 1000 mL beaker. This setup provides a larger surface area for the oil but still allows a low oil depth to be

maintained. Preliminary testing of the 31-point HV electrode in the fume hood in air at atmospheric pressure was carried out for oils a, b, and c. The next step is to test the corona reactor in a pressure vessel filled with a hydrogen rich gas to discover the overall viscosity change created by the corona discharge.

REFERENCES

[1] "International Energy Outlook 2014," ed: U.S. Energy Information Administration, 2014.

[2] (2010, 2014). Heavy oil unlocking the potential, Chevron Corporation. [Online]. 10. Available: http://www.chevron.com/documents/pdf/heavyOil.pdf

[3] J. Henderson and L. Weber, "Physical upgrading of heavy crude oils by the application of heat," *Journal of Canadian Petroleum Technology,* vol. 4, pp. 206-212, 1965.

[4] J. G. Speight, *The Chemistry and Technology of Petroleum*, 4th ed. Boca Raton, FL: Taylor & Francis, 2007.

[5] E. Kendall, "The electrical conductivity of medium heavy crude oil," *Journal of Canadian Petroleum Technology,* vol. 17, pp. 37-38, 1978.

[6] M. S. Rana, V. Sámano, J. Ancheyta, and J. A. I. Diaz, "A review of recent advances on process technologies for upgrading of heavy oils and residua," *Fuel,* vol. 86, pp. 1216-1231, Jun. 2007.

[7] D. Berry and D. Shekhawat. (2012, 2014). Non-thermal plasma for fossil energy related applications. [Online]. Available: http://www.netl.doe.gov/File%20Library/Research/On%20Site%20Research/R-D155.pdf

[8] A. Jaworek and A. Krupa, "Electrical characteristics of a corona discharge reactor of multipoint-to-plane geometry," *Czechoslovak Journal of Physics,* vol. 45, pp. 1035-1047, Dec. 1995.

[9] J. Chang, P. A. Lawless, and T. Yamamoto, "Corona discharge processes," *Plasma Science, IEEE Transactions on,* vol. 19, pp. 1152-1166, Dec. 1991.

[10] T. Paulmier and L. Fulcheri, "Use of non-thermal plasma for hydrocarbon reforming," *Chemical Engineering Journal,* vol. 106, pp. 59-71, 1/28/ 2005.

[11] A. Fridman, *Plasma Chemistry*. New York, NY: Cambridge University Press, 2008.

[12] F. F. Chen, *Introduction to Plasma Physics and Controlled Fusion*, 2nd ed. New York, NY: Springer Science+Business Media, 2006.

[13] H. Conrads and M. Schmidt, "Plasma generation and plasma sources," *Plasma Sources Science and Technology*, vol. 9, p. 441, Nov. 2000.

[14] Y. P. Raizer, *Gas Discharge Physics*. New York: Springer-Verlag, 1991.

[15] H. L. Chen, H. M. Lee, S. H. Chen, Y. Chao, and M. B. Chang, "Review of plasma catalysis on hydrocarbon reforming for hydrogen production—Interaction, integration, and prospects," *Applied Catalysis B: Environmental*, vol. 85, pp. 1-9, 12/17/ 2008.

[16] V. Nehra, A. Kumar, and H. Dwivedi, "Atmospheric non-thermal plasma sources," *International Journal of Engineering*, vol. 2, p. 53, 2008.

[17] A. Chirokov, A. Gutsol, and A. Fridman, "Atmospheric pressure plasma of dielectric barrier discharges," *Pure and applied chemistry*, vol. 77, pp. 487-495, Feb. 2005.

[18] B. R. Locke, M. Sato, P. Sunka, M. R. Hoffmann, and J. S. Chang, "Electrohydraulic discharge and nonthermal plasma for water treatment," *Industrial & Engineering Chemistry Research*, vol. 45, pp. 882-905, 2006.

[19] M.-w. Li, G.-h. Xu, Y.-l. Tian, L. Chen, and H.-f. Fu, "Carbon dioxide reforming of methane using DC corona discharge plasma reaction," *The Journal of Physical Chemistry A*, vol. 108, pp. 1687-1693, 2004.

[20] E. van Veldhuizen and W. Rutgers, "Corona discharges: fundamentals and diagnostics," *Invited paper, Proc. Frontiers in Low Temp. Plasma Diagn. IV, Rolduc, Netherlands*, pp. 40-49, 2001.

[21] M. Goldman, A. Goldman, and R. Sigmond, "The corona discharge, its properties and specific uses," *Pure Appl. Chem*, vol. 57, pp. 1353-1362, Jan. 1985.

[22] K. Annamalai and I. K. Puri, *Combustion Science and Engineering*. Boca Raton, FL: Taylor & Francis Group, LLC, 2007.

[23] D. Staack, " Non-thermal plasma reforming of liquid phase hydrocarbons using low energy nanosecond pulsed discharges," in *Atmospheric Pressure Weakly Ionized Plasmas for Energy Technologies, Flow Control and Materials Processing*, Princeton University, NJ, 2011.

[24] J. Chen and J. H. Davidson, "Model of the negative DC corona plasma: comparison to the positive DC corona plasma," *Plasma Chemistry and Plasma Processing*, vol. 23, pp. 83-102, Mar. 2003.

[25] G. Gillis, M. Varhaug, D. Ireson, M. Oristaglio, G. Pirie, R. Rottenberg, *et al.* Schlumberger Oilfield Glossary [Online]. Available: http://www.glossary.oilfield.slb.com/

[26] R. J. Kalivoda. (2011, 2014). Understanding the limits of ultrasonics for crude oil measurement. *Production Processing Handling* [Online]. 46-50. Available: http://www.fmctechnologies.com/en/MeasurementSolutions/BusinessHighlights/ArticleArchive.aspx

[27] H. Taghvaei, A. Jahanmiri, M. R. Rahimpour, M. M. Shirazi, and N. Hooshmand, "Hydrogen production through plasma cracking of hydrocarbons: effect of carrier gas and hydrocarbon type," *Chemical Engineering Journal*, vol. 226, pp. 384-392, 6/15/ 2013.

[28] "Energy Bandwidth for Petroleum Refining Processes," ed: U.S. Department of Energy, 2006, p. 40.

[29] P. C. Kong, B. A. Detering, J. D. Grandy, and L. D. Zuck, "Plasma processing of hydrocarbon," presented at the Electric Power 2007, Donald Stephens Convention Center, Chicago, IL, 2007.

[30] F. Holzer and B. Locke, "Influence of high voltage needle electrode material on hydrogen peroxide formation and electrode erosion in a hybrid gas–liquid series electrical discharge reactor," *Plasma Chemistry and Plasma Processing,* vol. 28, pp. 1-13, 2/1/ 2008.

[31] B. Kozlov and V. Solovygov, "Limit current of a multipoint corona discharge," *Technical physics,* vol. 51, pp. 821-826, Jul. 2006.

[32] L. C. Thanh, "Negative corona in a multiple interacting point-to-plane gap in air," *Industry Applications, IEEE Transactions on,* pp. 518-522, Mar. 1985.

[33] P. J. McKinney, J. H. Davidson, and D. M. Leone, "Current distributions for barbed plate-to-plane coronas," *Industry Applications, IEEE Transactions on,* vol. 28, pp. 1424-1431, 1992.

[34] K. Adamiak and P. Atten, "Simulation of corona discharge in point–plane configuration," *Journal of electrostatics,* vol. 61, pp. 85-98, Jun. 2004.

[35] A. Jaworek and A. Krupa, "Corona discharge from a multipoint electrode in flowing air," *Journal of Electrostatics,* vol. 38, pp. 187-197, Nov. 1996.

[36] I. Suarasan, L. Ghizdavu, I. Ghizdavu, S. Budu, and L. Dascalescu, "Experimental characterization of multi-point corona discharge devices for direct ozonization of liquids," *Journal of Electrostatics,* vol. 54, pp. 207-214, Feb. 2002.

[37] T. Q. Hoang, X. Zhu, L. L. Lobban, and R. G. Mallinson, "Effects of gap and elevated pressure on ethanol reforming in a non-thermal plasma reactor," *Journal of Physics D: Applied Physics,* vol. 44, p. 274003, 7/13/ 2011.

[38] Y. Yang, "Direct non-oxidative methane conversion by non-thermal plasma: experimental study," *Plasma Chemistry and Plasma Processing,* vol. 23, pp. 283-296, Jun. 2003.

[39] G. L. Weissler, "Positive and negative point-to-plane corona in pure and impure hydrogen, nitrogen, and argon," *Physical Review,* vol. 63, pp. 96-107, 2/1/ 1943.

[40] J. Chang, F. Pontiga, P. Atten, and A. Castellanos, "Corona discharge characteristics of narrow coaxial wire-pipe discharge tubes with gas flow," in *Industry Applications Society Annual Meeting, 1993., Conference Record of the 1993 IEEE*, Toronto, Canada, 1993, pp. 1887-1893.

[41] A. Abánades, E. Ruiz, E. M. Ferruelo, F. Hernández, A. Cabanillas, J. M. Martínez-Val, *et al.*, "Experimental analysis of direct thermal methane cracking," *International Journal of Hydrogen Energy*, vol. 36, pp. 12877-12886, Oct. 2011.

[42] T. Kondo, S. Sato, A. Matsumura, I. Saito, A. Machdo de Carvlhoz, and W. Ferraz de Souza, "Thermal cracking property of marlim vacuum residue," in *217th ACS National Meeting*, Anaheim, CA, 1999, pp. 182-187.

[43] O. O. Bello, B. T. Ademodi, S. R. A. Macaulay, and G. K. Latinwo, "Effects of operating conditions on compositional characteristics and reaction kinetics of liquid derived by delayed coking of nigerian petroleum residue," *Brazilian Journal of Chemical Engineering*, vol. 23, pp. 331-339, 2006.

[44] A. Jahanmiri, M. R. Rahimpour, M. Mohamadzadeh Shirazi, N. Hooshmand, and H. Taghvaei, "Naphtha cracking through a pulsed DBD plasma reactor: effect of applied voltage, pulse repetition frequency and electrode material," *Chemical Engineering Journal*, vol. 191, pp. 416-425, 5/15/ 2012.

[45] H. D. A. Honorato, R. C. Silva, C. K. Piumbini, C. G. Zucolotto, A. A. de Souza, A. G. Cunha, *et al.*, "1H low- and high-field NMR study of the effects of plasma treatment on the oil and water fractions in crude heavy oil," *Fuel*, vol. 92, pp. 62-68, Feb. 2012.

[46] G. Prieto, M. Okumoto, K. Takashima, S. Katsura, A. Mizuno, O. Prieto, *et al.*, "Nonthermal plasma reactors for the production of light hydrocarbon olefins from heavy oil," *Brazilian Journal of Chemical Engineering*, vol. 20, pp. 57-61, 2003.

[47] M. R. Khani, S. H. R. Barzoki, M. S. Yaghmaee, S. I. Hosseini, M. Shariat, B. Shokri, *et al.*, "Investigation of cracking by cylindrical dielectric barrier discharge reactor on the n-hexadecane as a model compound," *Plasma Science, IEEE Transactions on*, vol. 39, pp. 1807-1813, Sep. 2011.

[48] R. M. Renneke, L. A. Rosocha, and K. Yongho, "Temperature effects on gaseous fuel cracking studies using a dielectric barrier discharge," *Plasma Science, IEEE Transactions on,* vol. 36, pp. 2905-2908, Dec. 2008.

[49] L. A. Rosocha, K. Yongho, G. K. Anderson, L. Jae Ok, and S. Abbate, "Decomposition of ethane in atmospheric-pressure dielectric-barrier discharges: experiments," *Plasma Science, IEEE Transactions on,* vol. 34, pp. 2526-2531, Dec. 2006.

[50] L. Lobban and A. Marafi, "An investigation on the effects of corona discharge on ethane oxidative dehydration reaction," in *16th World Petroleum Congress*, Calgary, Canada, 2000, p. 40.

[51] B. E. van Heesch, G. Pemen, K. Yan, S. V. Van Paasen, K. J. Ptasinski, and P. A. Huijbrechts, "Pulsed corona tar cracker," *Plasma Science, IEEE Transactions on,* vol. 28, pp. 1571-1575, Oct. 2000.

[52] G. Prieto, M. Okumoto, K. Shimano, K. Takashima, S. Katsura, and A. Mizuno, "Reforming of heavy oil using nonthermal plasma," *Industry Applications, IEEE Transactions on,* vol. 37, pp. 1464-1467, 2001.

[53] G. Prieto, M. Okumoto, K. Shimano, K. Takashima, S. Katsura, A. Mizuno, *et al.*, "Heavy oil conversion by plasma chemical reactors," in *Industry Applications Conference, 1999. 34th IAS Annual Meeting. Conference Record of the 1999 IEEE*, 1999, pp. 1144-1149 vol.2.

[54] Y. Matsui, S. Kawakami, K. Takashima, S. Katsura, and A. Mizuno, "Liquid-phase fuel re-forming at room temperature using nonthermal plasma," *Energy & Fuels,* vol. 19, pp. 1561-1565, 2005.

[55] F. P. Miknis and R. W. Grimes, "Fossil fuel and hydrocarbon conversion using hydrogen-rich plasmas," Western Research Institute, Laramie, WY WRI-96-R008, 1996.

[56] J. L. Hueso, V. c. J. Rico, J. Cotrino, J. M. Jiménez-Mateos, and A. n. R. González-Elipe, "Water plasmas for the revalorisation of heavy oils and cokes from petroleum refining," *Environmental Science & Technology,* vol. 43, pp. 2557-2562, 2009.

[57] D. Yang, "Heavy oil upgrading from electron beam (e-beam) irradiation," M.S. thesis, Texas A&M University, College Station, TX, 2009.

[58] A. R. Hambley, *Electrical Engineering: Principles and Applications*, 4th ed. Upper Saddle River, NJ: Pearson Prentice Hall, 2008.

[59] R. Ohyama, K. Kaneko, J. Chang, x, and Shih, "Flow visualization and image analysis of gas-phase AC corona discharge induced electrohydrodynamic liquid flow in a stratified fluid," *Dielectrics and Electrical Insulation, IEEE Transactions on*, vol. 10, pp. 57-64, Feb. 2003.

[60] H. Kawamoto and S. Umezu, "Electrohydrodynamic deformation of water surface in a metal pin to water plate corona discharge system," *Journal of Physics D: Applied Physics*, vol. 38, p. 887, 3/21/ 2005.

[61] G. M. Bodner. (2014). *Properties of liquids* [Online]. Available: http://chemed.chem.purdue.edu/genchem/topicreview/bp/ch14/property.php#tension

[62] EIA. U.S. Crude Oil Composite Acquisition Cost by Refiners [Online]. Available: http://www.eia.gov/dnav/pet/hist/LeafHandler.ashx?n=PET&s=R0000___3&f=M

[63] EIA. Gasoline and Diesel Fuel Update [Online]. Available: http://www.eia.gov/petroleum/gasdiesel/

[64] IEA. (2012, 2014). IEA refinery margins, methodology notes. [Online]. *(September 2012)*. Available: http://omrpublic.iea.org/currentissues/user_guide.pdf

[65] A. Dehghani, M. Sattarin, H. Bridjanian, and K. Mohamadbeigy, "Investigation on effectiveness parameters in residue upgrading methods," *Pet. Coal*, vol. 51, pp. 229-236, 2009.

[66] A. Fridman, A. Chirokov, and A. Gutsol, "Non-thermal atmospheric pressure discharges," *Journal of Physics D: Applied Physics*, vol. 38, p. R1, 1/21/ 2005.

APPENDIX A: PRELIMINARY EXPERIMENTAL RESULTS ADDENDUM

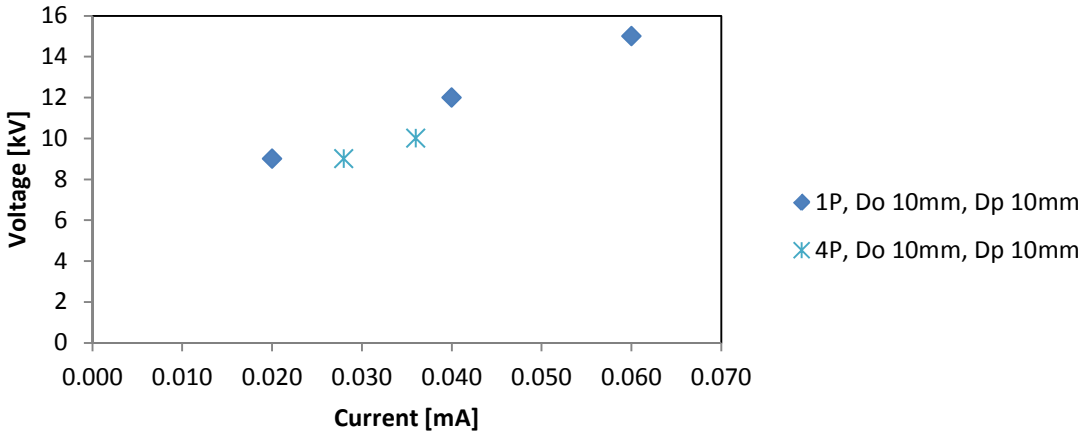

Figure 36: Current and voltage trend for various HV electrodes with D_o=10 mm and D_p=10 mm

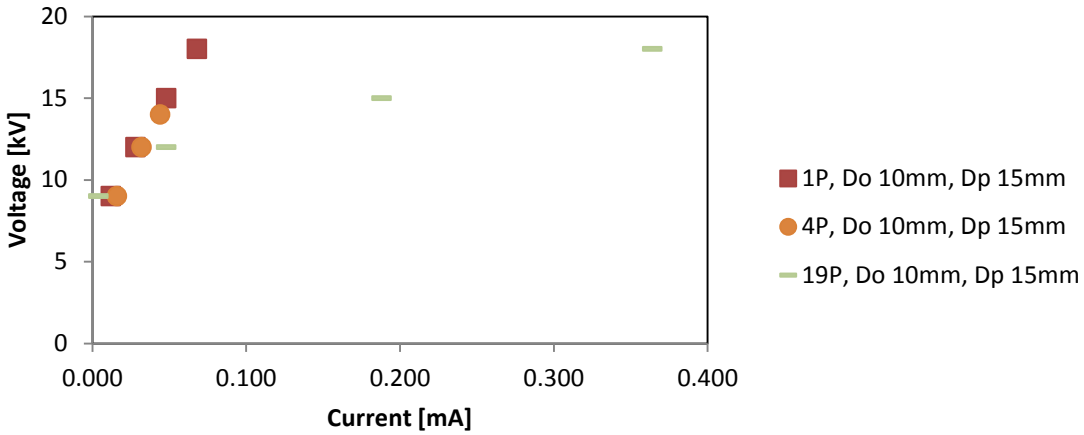

Figure 37: Current and voltage trend for various HV electrodes with D_o=10 mm and D_p = 15 mm

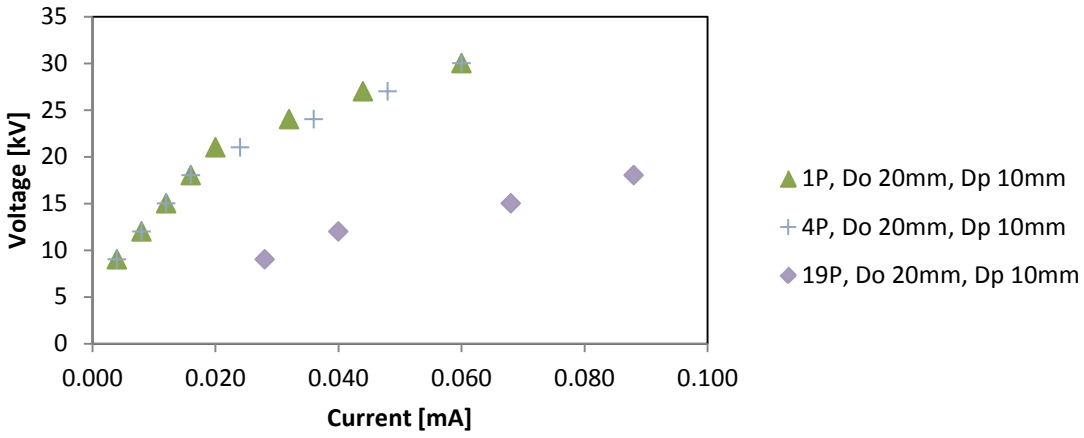

Figure 38: Current and voltage trend for various HV electrodes with D_o=20 mm and D_p=10 mm

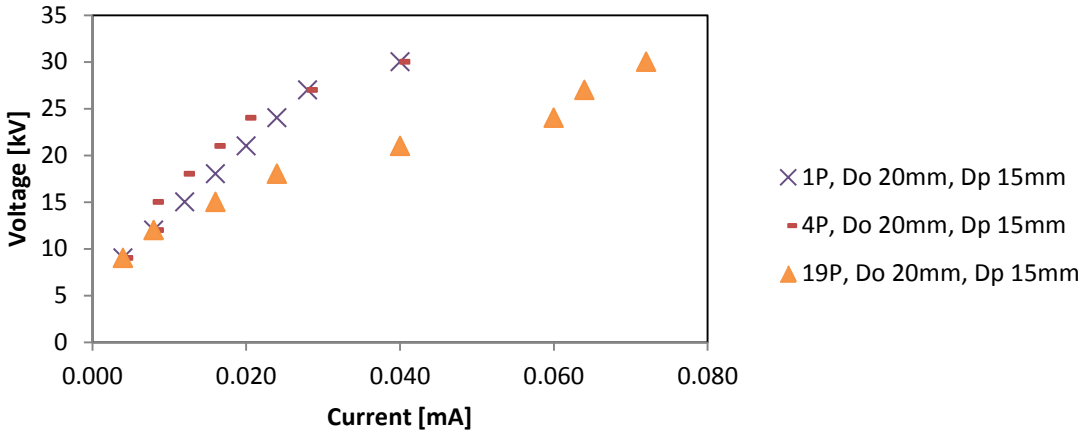

Figure 39: Current and voltage trend for various HV electrodes with D_o=20 mm and D_p=15 mm

APPENDIX B: CURRENT AND VOLTAGE CHARACTERISTICS DURING 4 HOUR CORONA TREATMENT OF OIL D

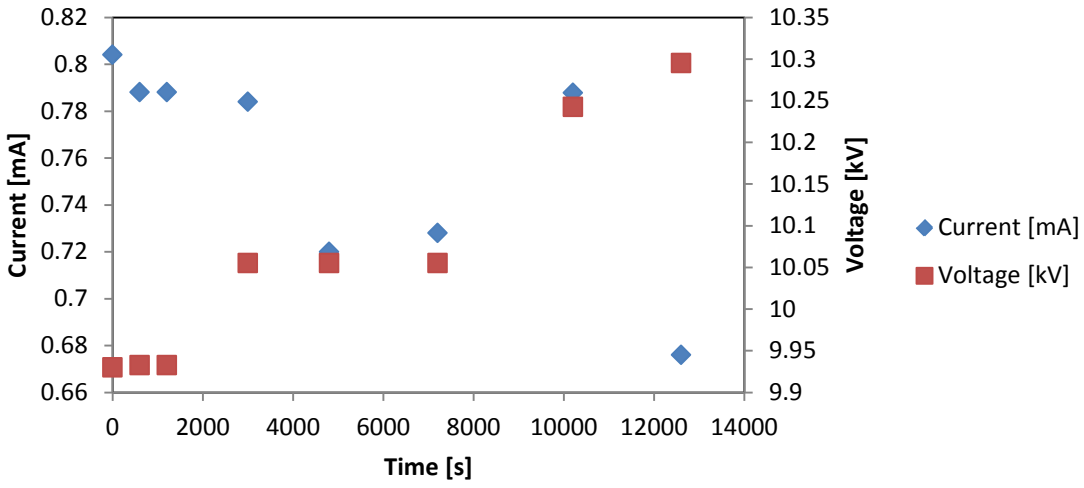

Figure 40: Test 2.11.14 current and voltage trend over time

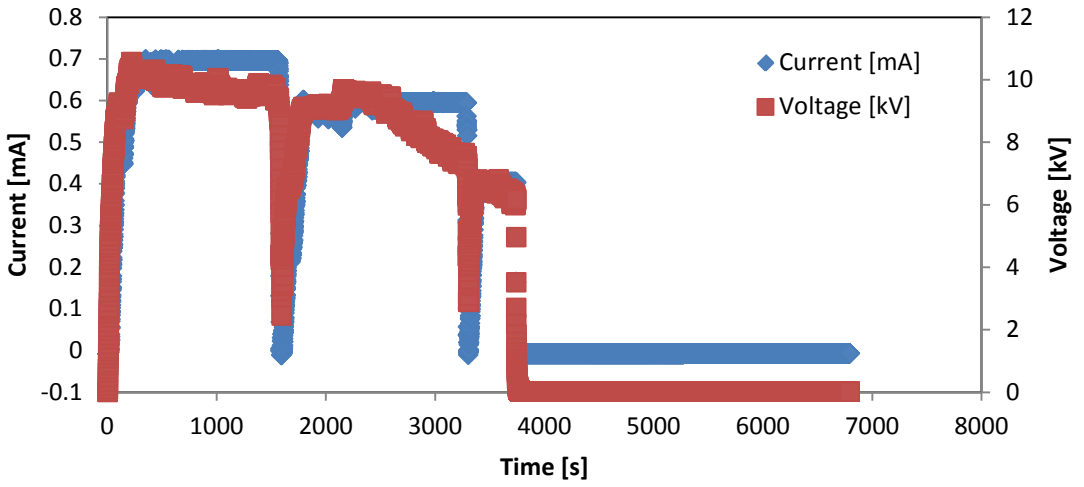

Figure 41: VoltCurMon_179 current and voltage trend over time

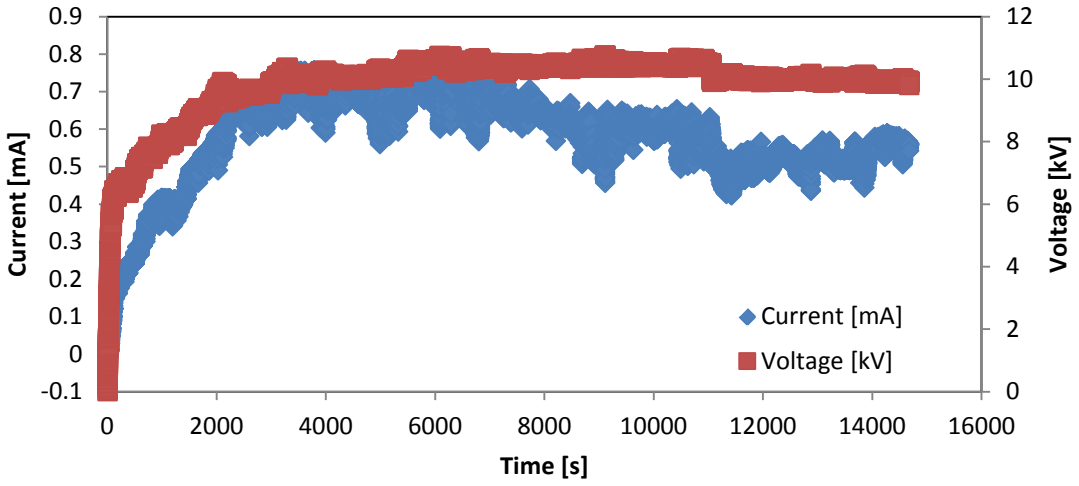

Figure 42: VoltCurMon_207 current and voltage trend over time

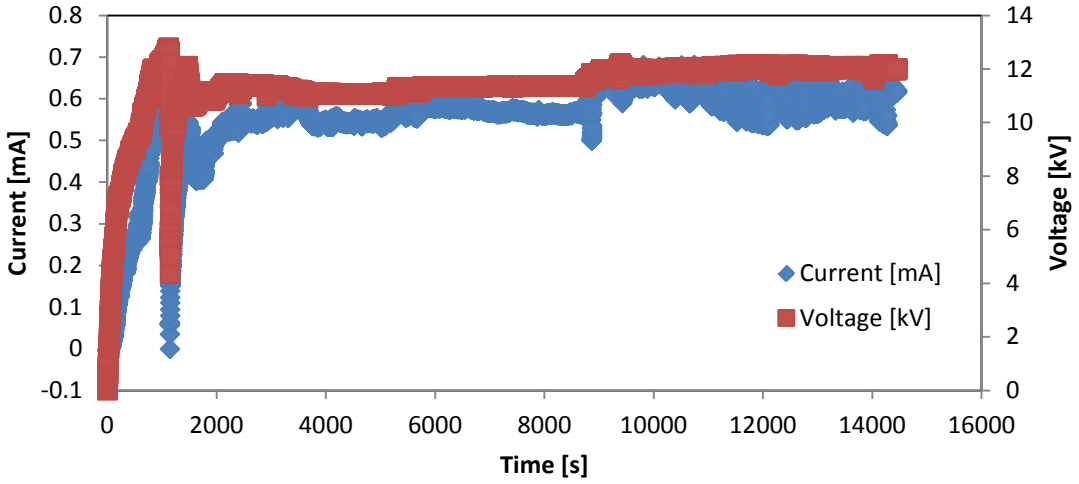

Figure 43: VoltCurMon_209 current and voltage trend over time

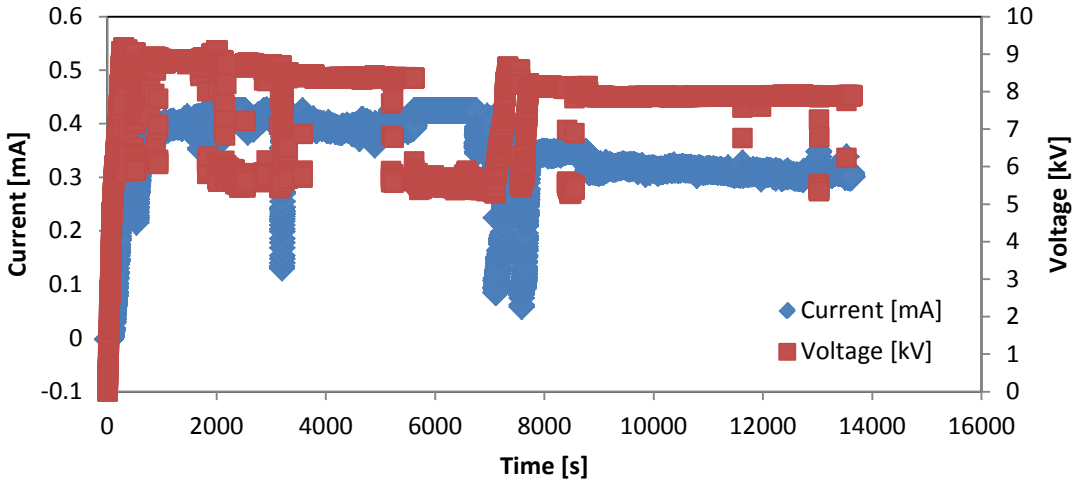

Figure 44: VoltCurMon_234 current and voltage trend over time

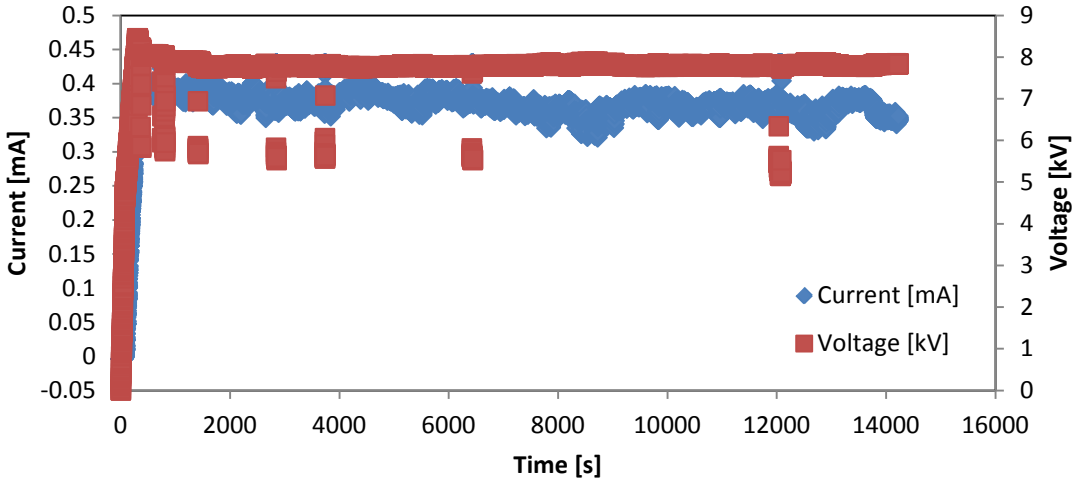

Figure 45: VoltCurMon_236 current and voltage trend over time

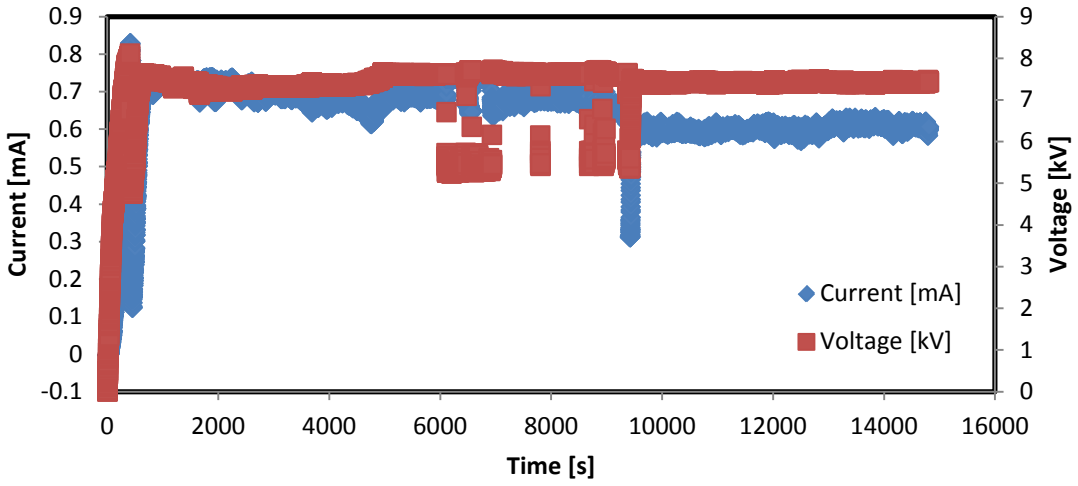

Figure 46: VoltCurMon_238 current and voltage trend over time

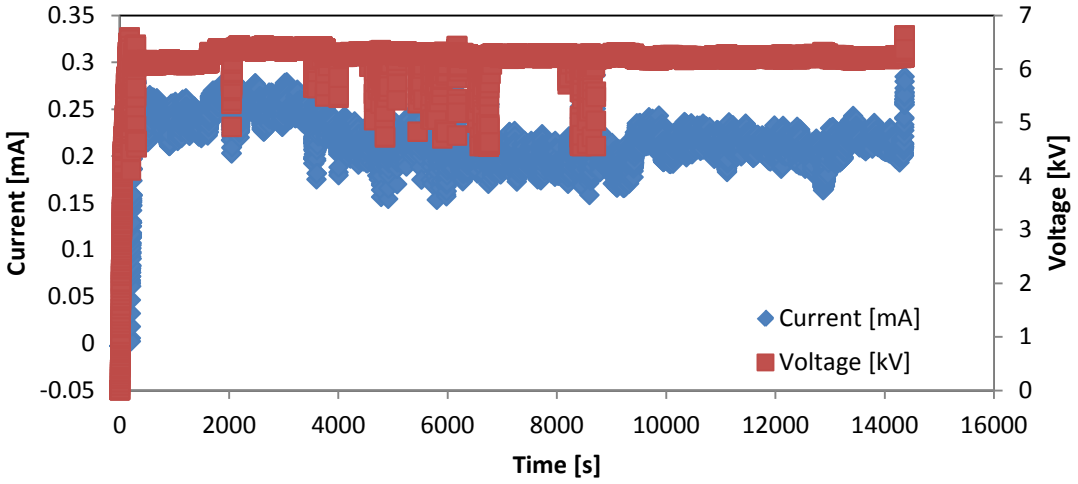

Figure 47: VoltCurMon_245 current and voltage trend over time

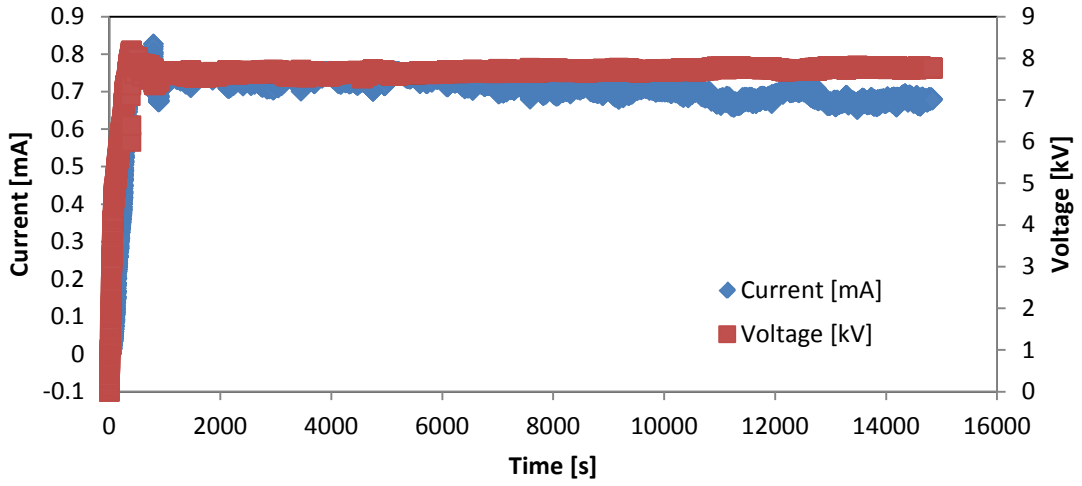

Figure 48: VoltCurMon_254 current and voltage trend over time

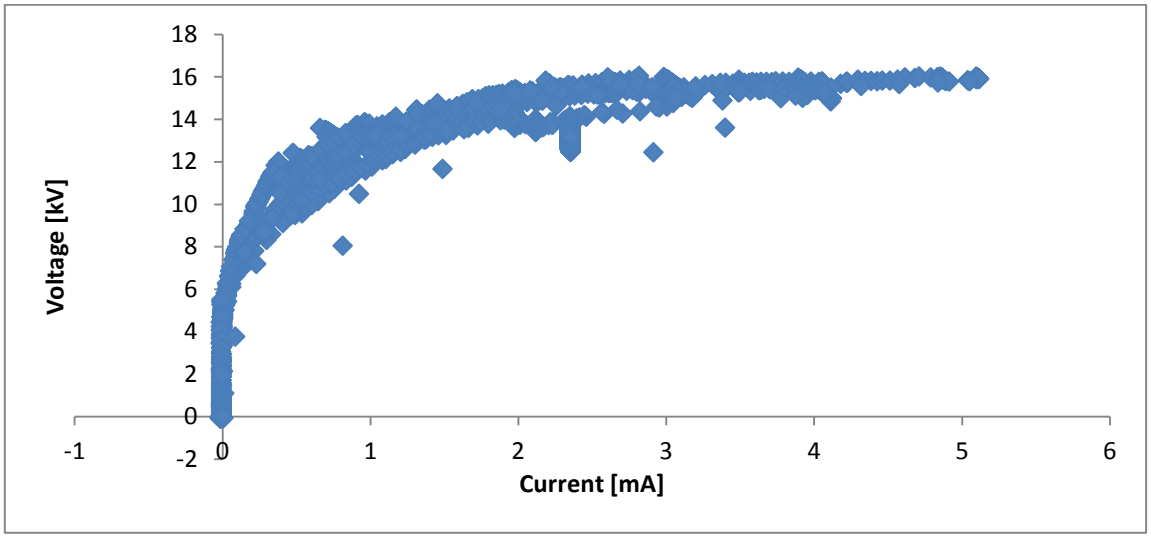

Figure 49: Current and voltage characteristics during 4 hour corona treatment of oil d with H_2 and CH_4 in the distillation tower (VoltCurMon_155)

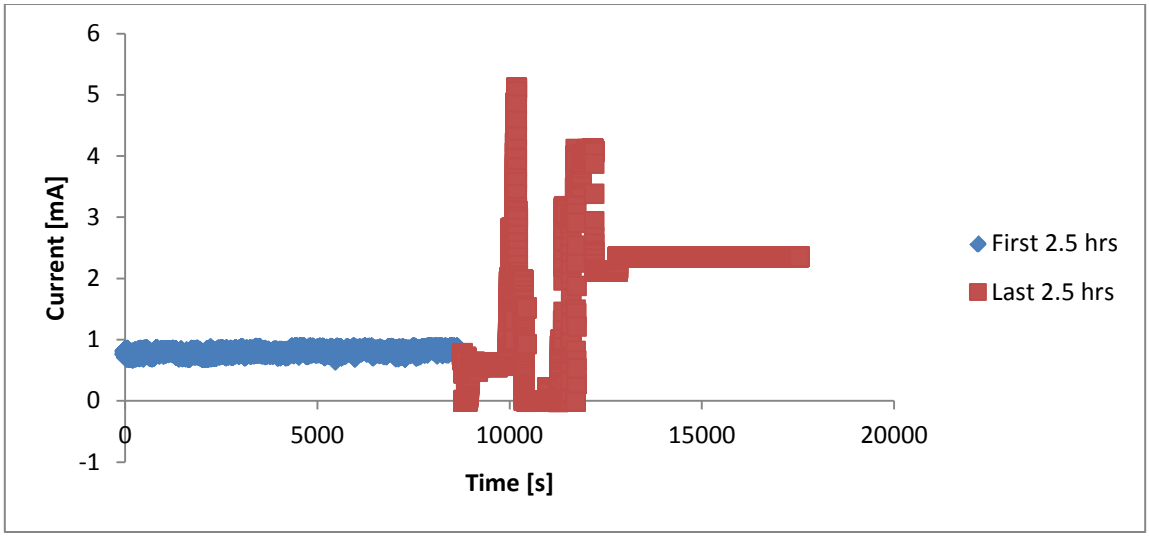

Figure 50: VoltCurMon_155 current trend over time

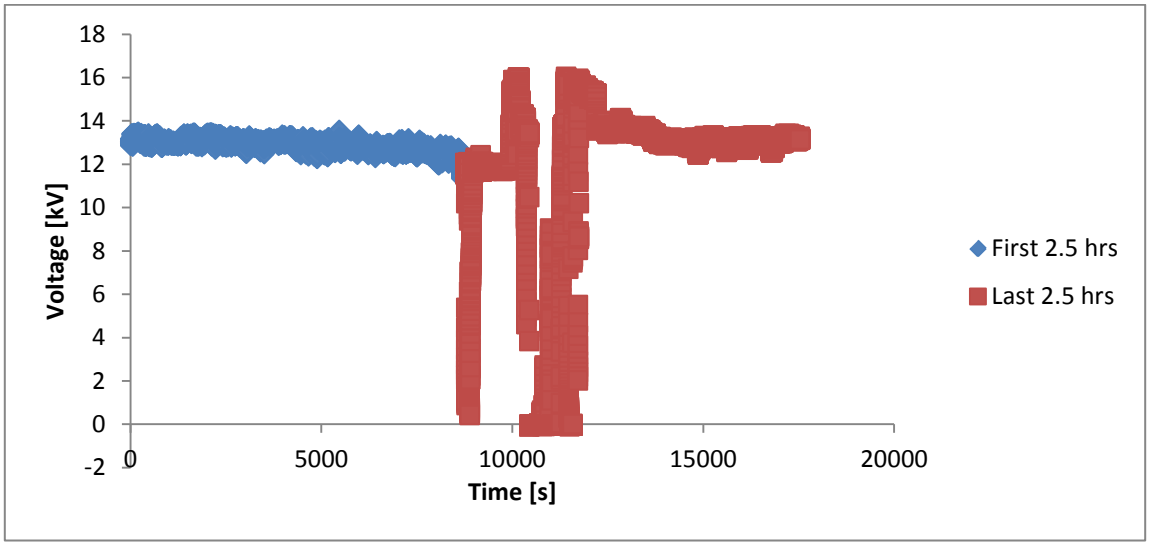

Figure 51: VoltCurMon_155 voltage trend over time

APPENDIX C: ADDITIONAL PRETESTS FOR DISTILLATION TOWER

Table 13: Average temperature of additional pretests for distillation tower

Test	VoltCurMon	T_1 [°F]	T_2 [°F]	T_3 [°F]	T_4 [°F]	T_5 [°F]	T_{HP} [°F]
6.4.14[a]	175-177	450	580	450	80	422	842
8.7.14	242	500	-	502.2	83.1	540.5	473

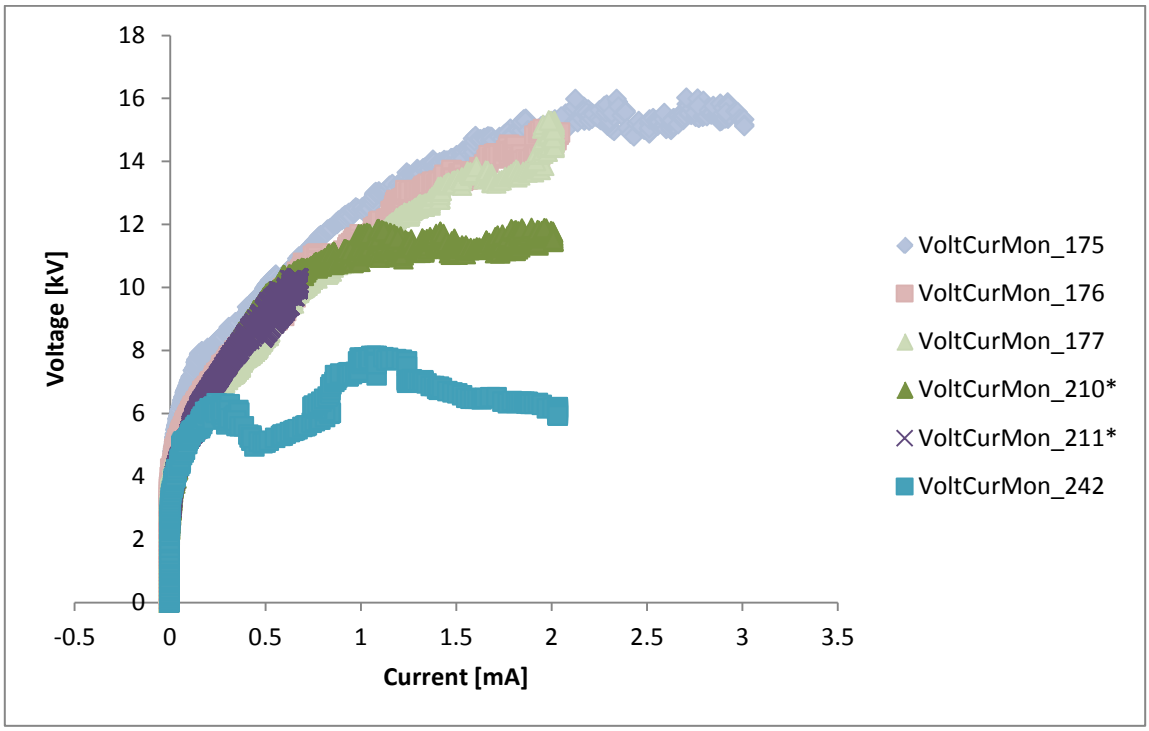

Figure 52: Additional pretests for determination of voltage and current characteristics of oil d with H_2 in the distillation tower

APPENDIX D: MALDI MS RESULTS[2]

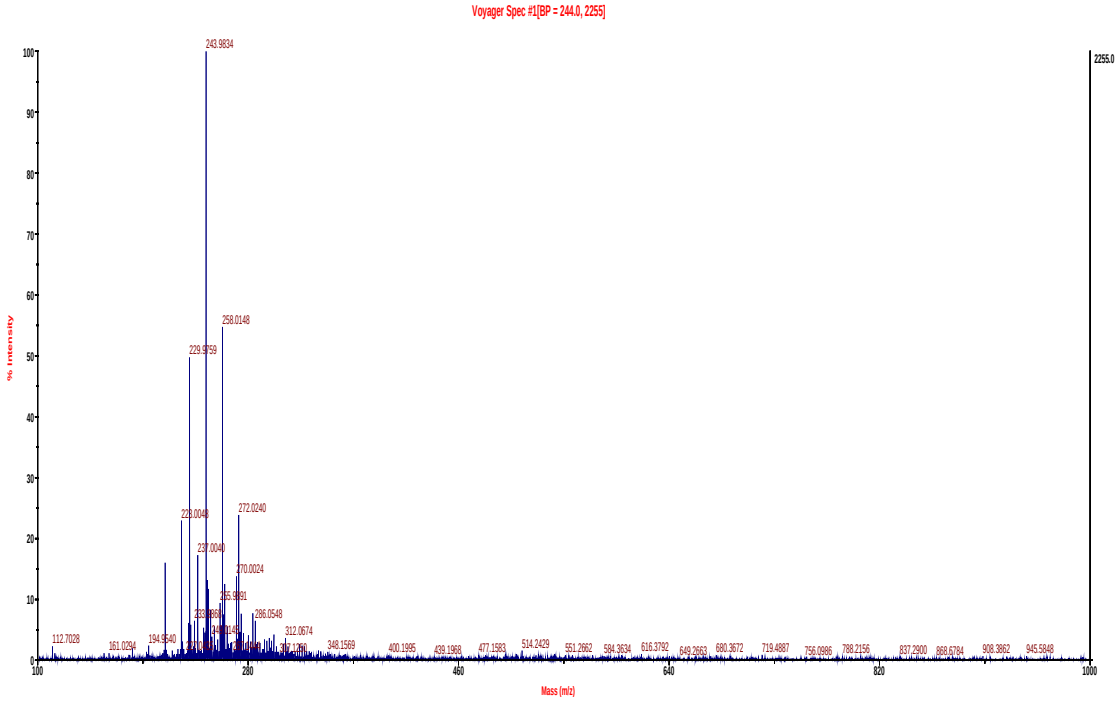

[2] Use of the TAMU/LBMS is acknowledged.

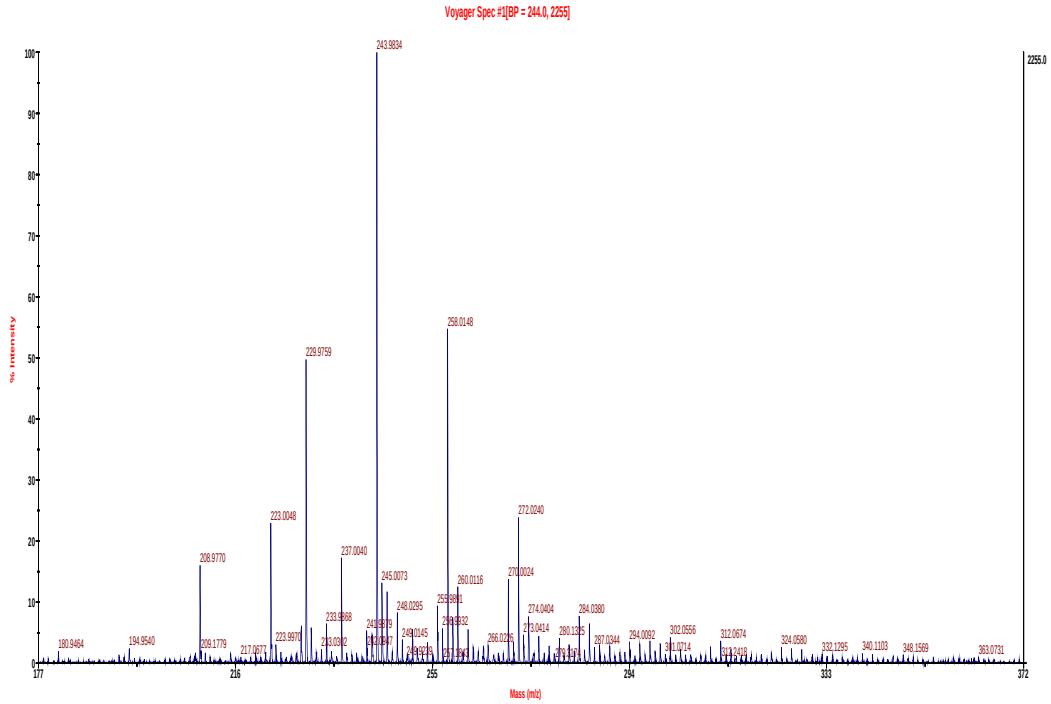
Voyager Spec #1[BP = 244.0, 2255]
% Intensity
Mass (m/z)
2255.0
243.9834
258.0148
229.9759
272.0240
223.0048
237.0040
208.9770
245.0073
260.0116
270.0024
248.0295
274.0404
284.0380
180.9464
194.9540
209.1779
217.0677
223.9970
233.9868
249.0145
266.0226
280.1325
294.0092
297.0344
302.0556
312.0674
324.0580
332.1295
340.1103
348.1569
363.0731